

**Journal:** ACP

**MS No.:** acp-2019-156

**MS Type:** Research article

**Title:** Observations of Highly Oxidised Molecules and Particle Nucleation in the Atmosphere of Beijing

**Author(s):** James Brean et al.

## RESPONSE TO REVIEWERS

We thank the reviewers for their very helpful comments and are pleased to respond.

### REVIEWER #1

L27: please define the used acronyms (VOC, BVOC)

**RESPONSE:** Definitions added.

L27: It would be good to mention already in the abstract when the data were taken (month and year).

**RESPONSE:** Dates added.

L37: "O<sub>3</sub> is lower on the days with higher HOM concentrations": This sounds as if O<sub>3</sub> inhibits the HOM formation. Can this just be coincidence as there are relatively few days of measurements?

**RESPONSE:** This is probably not O<sub>3</sub> inhibiting the formation, this just indicates that O<sub>3</sub> may not be as important an oxidant as OH. The wording here has been changed to better indicate this.

135: 3 sccm of carrier (sheath?) gas flow for N<sub>2</sub> is very low as this flow is typically on the order of 20 to 30 slm in CI-API-TOF instruments, please check. In addition, only one unit for the flows should be used (currently Lpm, sccm and SLM are used).

**RESPONSE:** Carrier flow refers to the small flow of N<sub>2</sub> across the surface of liquid HNO<sub>3</sub>, carrying HNO<sub>3</sub> through to the inlet to produce NO<sub>3</sub><sup>-</sup>. This has been reworded for clarity and the rest of the units have been fixed.

L145: Usually the nitric acid trimer (m/z 188, i.e., (HNO<sub>3</sub>)<sub>2</sub>NO<sub>3</sub> – ) yields a rather high signal in nitrate CI-API-TOF spectra, too. If this signal is not observed it points to rather strong fragmentation of cluster ions. Is the trimer signal missing completely? Furthermore, it is mentioned here that all signals are normalized with the primary ion count rates; however, in the figures this normalization seems to be missing. The statement here also contradicts the statement in

**RESPONSE:** The trimer signal is present in these spectra, just relatively small compared to these other reagent ion peaks, so would make a relatively small change to this normalization, and there are other occasional peaks which appear within one full-width-half-maximum of the peak at 188, causing some uncertainty in the signal intensity.

L149/150 ("... all values are reported in signal intensity, ions/s."). Rather than reporting signal intensity (ions/s) I highly recommend to report normalized signals in all figures, i.e., the data should be normalized by the sum of all primary ions (m/z 62, 80, 125 and 188, if present). It would also be good to mention that the conversion constant (from normalized counts to concentrations) is typically between a few 10<sup>9</sup> and 1×10<sup>10</sup> molecule cm<sup>-3</sup> (see e.g., Kürten et al., 2012). In this way the reader can get an idea of the rough HOM and sulfuric acid concentrations. One further suggestions relates to the fact, that concentrations of SO<sub>2</sub> and OH were measured along with the condensation sink. From these data the H<sub>2</sub>SO<sub>4</sub> concentration can be estimated (using a simple steady-state assumption for the main source and the sink of H<sub>2</sub>SO<sub>4</sub>). In this way, an estimate for the calibration constant can be derived.

**RESPONSE:** This was a mislabelling of the axes. All of these signals have been normalised to reagent ion counts of 1e+5 and this has been fixed on all figures. Unfortunately the OH, HO<sub>2</sub> and RO<sub>2</sub> data have very

little temporal overlap with our own (discussed below) so the resultant H<sub>2</sub>SO<sub>4</sub> proxy had very little crossover with our own values. Values of the calibration constant have been calculated from the very limited data available and are now included.

L150: It would be good to mention typical values for the mass resolving power and mass accuracy.

**RESPONSE:** These have been added (3500 m/dm, 20ppm @ 288 m/Q).

L165/166: Please swap the order of the reported size ranges as the LongSMPS is mentioned before the NanoSMPS.

**RESPONSE:** Fixed.

L168 and L170: The term “saturator pressures” is used here; however, in the PSM the saturator flow rates are varied in order to achieve different diethylene glycol supersaturations; this should be clarified.

**RESPONSE:** Fixed. This should have read saturator flows.

L172: It is not clear what is meant by “similar behavior of the upper and two lower size cuts”. Do the authors mean that the concentrations for the lower and upper two size channels typically correlate very well?

**RESPONSE:** Each member of the two smaller (<1.3 and 1.36 nm) and two larger (1.67 and 2.01 nm) correlated well and also provided data of near identical magnitudes, so the average of these were taken to produce just one single dN/dlogdp value.

L187: It is mentioned that OH, RO<sub>2</sub> and HO<sub>2</sub> concentrations were measured, yet, none of these data are shown. To my knowledge the present study is the first ambient study where HOM, O<sub>3</sub>, OH, HO<sub>2</sub> and RO<sub>2</sub> were measured simultaneously. Therefore, a lot could be learned about the different HOM formation pathways (e.g., if certain HOM originate rather from reactions with OH or O<sub>3</sub>). It would be great if somehow the HO<sub>x</sub> data could be incorporated in the data analysis.

**RESPONSE:** Unfortunately the FAGE data was only coincidental with a small amount of the CIMS data. There is about 19 hours of overlapping data on 21/06/2017, and a few hours on 23/06 and overnight on 24/06/2017 – 25/06/2017. As this data is sparse, we felt it was not enough to add any meaningful interpretation of our own data.

Figure S1: please show the (normalized, see comment above) H<sub>2</sub>SO<sub>4</sub> signals on a log scale

**RESPONSE:** This has been fixed. NO and NO<sub>2</sub> are now also on log scales.

L209: delete one of the “that”

**RESPONSE:** Removed.

L221: I think some of the signals cannot be unambiguously identified, e.g., the mentioned sum formula could also be written as C<sub>5</sub>H<sub>8</sub>O<sub>2</sub>(HNO<sub>3</sub>)<sub>2</sub> or C<sub>5</sub>H<sub>9</sub>NO<sub>5</sub>(HNO<sub>3</sub>), where the HNO<sub>3</sub> could be coming from the charger ions (i.e., (HNO<sub>3</sub>)<sub>2</sub>NO<sub>3</sub> – or (HNO<sub>3</sub>)NO<sub>3</sub> – rather than NO<sub>3</sub> – ). One way to test this hypothesis is to check if the m/z 288 signals correlates with m/z 225 (this could be the same neutral molecule just with one less HNO<sub>3</sub> from the charging process). I also think that this possibility of ambiguity exists for some other nitrogen containing species, which affects the evaluation of the oxidation state values shown in Figure 1. Although the question of ambiguity cannot be ultimately resolved it should be mentioned and discussed briefly.

**RESPONSE:** Checking all of these signals was part of our analyses. None of these peaks correlated with their nitrate monomer/dimer/trimer counterparts. If some of our formulae were to exist as clusters with

the nitrate dimer, it would follow that their cluster with the nitrate monomer would be seen 63 m/Q lower with a much higher signal, and these two species would correlate well.

L245/246: Schobesberger et al. (2015) provide a detailed list of observed signals in the nucleating system of sulfuric acid and ammonia. From their observations prominent signals for 3 the reported masses (m/z 344 and m/z 362) seem rather unlikely. I would also be surprised if just these two mixed ammonia-sulfuric acid peaks show up in the spectra without any others. Have the authors considered the isotopic distributions of the assigned signals in their analysis? Sulfur has a distinct isotopic pattern; therefore, the assigned formulas in Table S2 for the sulfur containing species could be checked by considering the isotopes.

**RESPONSE:** Isotopes were considered for all peaks; however, these peaks have been removed from this analysis as they would likely not exist in the absence of smaller peaks of similar composition (see more detail below). These reference points have been replaced with reference to SA-DMA clusters.

L267/268: As mentioned before, it would be great if more information on HOx and RO2 could be provided.

**RESPONSE:** See above.

L295: the plot does not show concentrations but the raw signals L344: J(O1D) is not shown in Figure S1

L347: neither O3 nor HOM are shown in Figure S2

**RESPONSE:** This has been fixed.

L410: in the PSM particles are grown within the condenser

**RESPONSE:** Corrected.

L411 and L412: Can the authors at least speculate what compounds cause these signals? If they are from (in)organic compounds (H2O, NH3, H2SO4 and maybe amines) the number of possible combinations should not be too large.

**RESPONSE:** This has been amended. Signal intensity for these peaks was extremely low and over-represented due to the normalisation that had been applied so this section was discarded. These figures had been amended but the text had not.

L420 to 430: The possibility of sulfuric acid-amine nucleation should be further discussed. To me it seems very unlikely that only selected SA-DMA clusters show up in the spectra. For nitrate CI-API-TOF measurements a detailed study of sulfuric acid-dimethylamine clusters has recently been presented (Kürten et al., 2014). That study has also shown that DMA together with sulfuric acid forms new particles very efficiently; therefore, tiny amounts (pptv) should suffice for efficient nucleation and the presence of DMA in clusters is already evidence that DMA is assisting in NPF. I suggest to search for further DMA (or other amine) containing clusters and to check if ambiguity can be ruled out, e.g., that the clusters with DMA and sulfuric acid are not due to some other (organic) compound. This can be done by taking into account the isotopic patterns. In addition, in Table S2 one of the listed clusters is C2H7NHSO4<sup>-</sup> (i.e., a C2-amine clustered with the bisulfate ion). This cluster does, however, not exist as the Lewis base (HSO4<sup>-</sup>) does not form a stable cluster with a strong base (C2-amine) unless at least two further acids (H2SO4) are present in the cluster (Ortega et al., 2014; Kürten et al., 2014).

**RESPONSE:** Peaks that were assigned SA-DMA clusters were very small (and often on the shelves of larger peaks). The isotope patterns were considered but these isotopic peaks were even smaller. The assigned SA-DMA clusters may have been misassigned previously as we are also dubious about the presence of peaks with multiple SA, ammonia and water molecules, while smaller SA-NH3 peaks are not present. However, reconsidering the mass spectra has yielded a handful of useful SA-DMA peaks. Some are still lost to shelves of other peaks and some others are not present. Peaks include C2H7N(H2SO4)2HSO4<sup>-</sup>, (C2H7N)2(H2SO4)2HSO4<sup>-</sup>, and (C2H7N)2(H2SO4)3HSO4<sup>-</sup> and have been added to the peak list, and these correlate

well with each other, as well as sulfuric acid monomer and dimer. SA-NH<sub>3</sub> peaks are not present. We have added to and edited the manuscript accordingly.

Figure 2: Is this MD plot corresponding to a period when NPF is occurring? It would be good to show a second MD plot for another day (same time of day) when no NPF is occurring just to see what signals could make the difference. In addition, there seem to be really prominent peaks (negative MD) at m/z of ~500 and ~700. Have the corresponding compounds been identified? Do these signals show a distinct diurnal pattern with higher concentrations during NPF?

**RESPONSE:** The mass defect plot in the manuscript was initially for the nucleation period across the day of 25/06. This has been amended and the figure now shows the daytime period 10:30 – 12:00 on 25/06 to show a nucleation period, and 23/06 in a non-nucleation period. The HOMs + sulfuric acid monomer show the most significant increase between these two periods, most markedly <400 m/Q.

## REVIEWER #2

L26: VOC abbreviation in the abstract is not defined

**RESPONSE:** Added.

L28-31: sentence is hard to read

**RESPONSE:** Reworded.

L 58. Delete 'the' before 'many'

**RESPONSE:** Fixed.

L76: Add a “, the” after compound

**RESPONSE:** There is no mention of the word “compound” on L76, and this would not make sense on any other word in this paragraph?

L77: Abbreviate BVOC here. Biogenic should compare with anthropogenic VOCs. So correct these statements.

**RESPONSE:** Corrected.

L87-88: Statement is not clear.

**RESPONSE:** Reworded. The point of the statement is that the size and oxygen containing functionalities found in HOMs result in low and extremely low vapour pressures.

L129: change “organics” to “organic compounds”

**RESPONSE:** Fixed

L111: what is APHH here?

**RESPONSE:** Air Pollution and Human Health in a Developing Megacity. This has been added.

L179: what is it stand for d’p and Nd’p here? L186: What is J(O’D)?? Please provide some baseline information here.

**RESPONSE:** d’p is the diameter of the particle, Nd’p is the number of particles at diameter d’p. These have been added, J(O<sup>1</sup>D) is the photolysis rate of ozone, but references to this were erroneous and have been removed.

L244-258: This text is not clear enough to understand the Figure 2. Some background information should be provided how to interpret the data and what is observed followed by what does it mean?

**RESPONSE:** The background information is to be found in the figure caption, but this has also been added to the main body of text.

L261: change 'throw light upon' with 'reveal'

**RESPONSE:** Changed.

L263: peak in the daytime? But it looks from Figure 3 that mostly peaking in the evening/night time. Why there is no peak on 23-24/06/2017

**RESPONSE:** On 24/05 this peak is to be found in the afternoon. On the subsequent day there are two peaks (one just before midday, one shortly afterwards). We regarded all of these as daytime peaks. We presume the reviewer means 22/06-23/06? Light intensity was significantly lower on these two days than on other days of measurement, and temperatures were lower also, so both OH<sup>•</sup> would be lower, and lower temperatures limit the rates of autoxidation.

L268: HOM components peaking in the daytime? From Figure 3, it is not clear. What is the basis for this assumption that HOMs are produced by the oxidation of anthropogenic/biogenic components (e.g., alkylbenzenes, monoterpenes, isoprene).

Figure 3: C6 - C9 components, and summed C11 - C18 components, assumed to be dominated by alkylbenzenes and other larger components respectively-how this was assumed?

**RESPONSE:** The compounds were grouped by both their molecular formulae, as the HOM products of the oxidation of, for example, xylenes have been studied in flow tubes (forming largely compounds of formulae C<sub>8</sub>H<sub>12</sub>O<sub>x</sub>) and are therefore known. Aromatics like alkylbenzenes, as well as naphthalene and biphenyl, alongside isoprene and monoterpenes are currently the only molecules known to produce HOM. We also know the abundances of alkylbenzenes, monoterpenes, isoprene and other VOCs from PTR-MS. Earlier in the campaign and not coincidental with our CI-API-ToF data, GC and 2DGC VOC data were collected and these were also used to take a broad view on the relative abundances of different VOCs with the same mass (ie, how much limonene as compared to alpha-pinene, or how much ethylbenzene vs xylenes, with xylenes having significantly higher HOM yields). This information was used to conclude that alkylbenzenes, monoterpenes and isoprene produce most of the observed HOM, and further to link individual HOM to their precursor VOCs.

C11-18 compounds were assigned as individual oxidation products of single larger VOC rather than the dimers of smaller RO<sub>2</sub> molecules due largely to their C:H ratios being small, and indicative of aromatic precursors, and secondarily due to the small fraction of dimers seen of, for example, monoterpene oxidation products. Further to this, although fragmentation upon reaction with OH, or even upon secondary reaction with O<sub>3</sub> in the case of molecules with multiple double bonds like limonene occurs and can produce products with lower carbon numbers (ie, C<sub>9</sub>H<sub>14</sub>O<sub>x</sub> can either be a product of mesitylene oxidation or monoterpene oxidation), the bulk of these signals seemed not to come from fragmentation as what could be assigned as a possible fragment tended to always correlate poorly with both the VOC from which it would have fragmented, and the other oxidation products of that VOC.

L 284: Please add panels 'a, b, and c' in Figure 3 and accordingly refer these in the discussion in the manuscript here.

**RESPONSE:** This has been added.

L312: Relative to what??

**RESPONSE:** The relative ratios of  $C_8H_{10}O_n$  where  $n=5,6,7...$  This has been reworded for clarity.

L320: majority of peaks occurring the daytime? But from Figure 3, it is mostly in evening time.

**RESPONSE:** See above, the actual peaks are specified.

L336: Early afternoon peak? By looking at Figure 4, it looks like evening hrs. The scale showed '0:00 HRS' – Is it 24:00 hr?

**RESPONSE:** 00:00 is midnight. This is referring to the HOM peak, which is at 16:00 on 24/06 and 15:00 on 25/06. Early afternoon is probably an incorrect choice of wording here, this has been amended.

L337-338: From where, it is inferred this (i.e., similar behaviour of C3-benzenes and their oxidation products as C2-benzenes and their HOMs)?

**RESPONSE:** We have reworded this to clarify.

L344: I could not find J(O'D) in Figure S1!

**RESPONSE:** J(O<sup>1</sup>D) data was removed in an earlier version of this paper, this reference was erroneous.

L346-347: Figure S2 does not provide this information, please double check and maintain consistency between text and supplementary information.

**RESPONSE:** This has been fixed.

L350: This is inferred from which figure, please mention

**RESPONSE:** Figure 3b, this has been added.

L369: text is unclear-'what is unit mass data'

**RESPONSE:** Unit mass refers to mass spectral peak area data integrated over the whole of one unit mass, producing less complicated low resolution data.

L371-372: This normalization part is not clear enough to follow the figure 5. Please elaborate.

**RESPONSE:** Reworded for clarity.

L403-404: sentence is not clear. In Figure 3, point the two peak of HOMs on 25/06/2017 to understand the text described here.

**RESPONSE:** This has been streamlined and better explained in the text.

L405: I am not able to see the two peaks in C2-benzenes in Figure 4. Please encircle or write clearly to maintain consistency with figure.

**RESPONSE:** This was an erroneous reference and has been amended.

L407-9: These sentences are not clear. Please consider rephrasing these sentences

**RESPONSE:** Done.

L412: From Figure 5, PSM cluster peaked at 10:00 and 13:00 h have m/Q between 200-550 (as also stated on L409). But the specified m/Q here is beyond the scale shown in Figure 5. Is it correct or I am missing something.

**RESPONSE:** This has been amended. Signal intensity for these peaks was extremely low and over-represented due to the normalisation that had been applied so this section was discarded. These figures had been amended but the text had not.

L412: Add 'because of' after 'presumably'

**RESPONSE:** [See above.](#)

L416- 418: Please refer to the figure.

**RESPONSE:** [These figures are referred to above.](#)

L425: Define 'SA-DMA' here.

**RESPONSE:** [Added.](#)

L443: From the Figure 3, HOM peaked in the evening hours on 24/06/2017 compared to 25/06/2017, where HOM peaked at the early afternoon. So 'daytime peak of HOMs' need to be rephrased

**RESPONSE:** [This has been rephrased.](#)

1                   **OBSERVATIONS OF HIGHLY OXIDISED**  
2                   **MOLECULES AND PARTICLE NUCLEATION**  
3                   **IN THE ATMOSPHERE OF BEIJING**

4  
5                   **James Brean<sup>1</sup>, Roy M. Harrison<sup>1\*†</sup>, Zongbo Shi<sup>1</sup>**  
6                   **David C.S. Beddows<sup>1</sup>, W. Joe F. Acton<sup>2</sup> and**  
7                   **C. Nicholas Hewitt<sup>2</sup>, Freya A. Squires<sup>3</sup> and James Lee<sup>3</sup>**  
8  
9

10                   <sup>1</sup>**Division of Environmental Health and Risk Management,**  
11                   **School of Geography, Earth and Environmental Sciences**  
12                   **University of Birmingham**  
13                   **Edgbaston, Birmingham B15 2TT**  
14                   **United Kingdom**

15  
16                   <sup>2</sup>**Lancaster Environment Centre**  
17                   **Lancaster University, Lancaster LA1 4YQ**  
18                   **United Kingdom**

19  
20                   <sup>3</sup>**National Centre for Atmospheric Science**  
21                   **Wolfson Atmospheric Chemistry Laboratory**  
22                   **University of York, York YO10 5DD**  
23                   **United Kingdom**  
24

---

\* To whom correspondence should be addressed.  
Tele: +44 121 414 3494; Fax: +44 121 414 3709; Email: r.m.harrison@bham.ac.uk

†Also at: Department of Environmental Sciences / Center of Excellence in Environmental Studies, King Abdulaziz University, PO Box 80203, Jeddah, 21589, Saudi Arabia



25 **ABSTRACT**

26 Particle nucleation is one of the main sources of atmospheric particulate matter by number, with new  
27 particles having great relevance for human health and climate. Highly oxidised multifunctional  
28 organic molecules (HOMs) have been recently identified as key constituents in the growth, and,  
29 sometimes, in initial formation of new particles. While there have been many studies of HOMs in  
30 atmospheric chambers, flow tubes and clean environments, analyses of data from polluted  
31 environments are scarce. Here, measurements of HOMs and particle size distributions down to small  
32 molecular clusters are presented alongside volatile organic compounds (VOC) and trace gas data from  
33 a campaign in June 2017, in Beijing. Many gas phase HOMs have been characterised and their  
34 temporal trends and behaviours analysed in the context of new particle formation. The HOMs  
35 identified have a comparable degree of oxidation to those seen in other, cleaner, environments, likely  
36 due to an interplay between the higher temperatures facilitating rapid hydrogen abstractions and the  
37 higher concentrations of NO<sub>x</sub> and other RO<sub>2</sub> terminators ending the autoxidation sequence more  
38 rapidly. Our data indicate that alkylbenzenes, monoterpenes, and isoprene are important precursor  
39 VOCs for HOMs in Beijing. Many of the C<sub>5</sub> and C<sub>10</sub> compounds derived from isoprene and  
40 monoterpenes have a slightly greater degree of average oxidation state of carbon compared to those  
41 from other precursors. Most HOMs except for large dimers have daytime peak concentrations,  
42 indicating the importance of OH· chemistry in the formation of HOMs, as O<sub>3</sub> tends to be lower on  
43 days with higher HOM concentrations, ~~as O<sub>3</sub> is lower on the days with higher HOM concentrations;~~  
44 similarly, VOC concentrations are lower on the days with higher HOM concentrations. The daytime  
45 peaks of HOMs coincide with the growth of freshly formed new particles, and their initial formation  
46 coincides with the peak in sulfuric acid vapours, suggesting that the nucleation process is sulfuric  
47 acid-dependent, with HOMs contributing to subsequent particle growth.

48

49

## 50 1. INTRODUCTION

51 Atmospheric particle nucleation, or the formation of solid or liquid particles from vapour phase  
52 precursors is one of the dominant sources of global aerosol by number, with primary emissions  
53 typically dominating the mass loadings (Tomasi et al., 2016). New particle formation (NPF) or the  
54 secondary formation of fresh particles is a two-step process comprising of initial homogeneous  
55 nucleation of thermodynamically stable clusters and their subsequent growth. The rate of growth  
56 needs be fast enough to out-compete the loss of these particles by coagulation and condensation  
57 processes in order for the new particles to grow, and hence NPF is a function of the competition  
58 between source and sink (Gong et al., 2010). New particle formation has been shown to occur  
59 across a wide range of environments (Kulmala et al., 2005). The high particle load in urban  
60 environments was thought to suppress new particle formation until measurements in the early 2000s  
61 (McMurry et al., 2000; Shi et al., 2001; Alam et al., 2003), with frequent occurrences observed even  
62 in the most polluted urban centres. NPF events in Beijing occur on about 40% of days annually,  
63 with the highest rates in the spring (Wu et al., 2007, 2008; Wang et al., 2016). Chu et al. (2019)  
64 review ~~the~~ many studies of NPF which have taken place in China and highlight the need for long-  
65 term observations and mechanistic studies.

66  
67 NPF can lead to production of cloud condensation nuclei (CCN) (Wiedensohler et al., 2009; Yu and  
68 Luo, 2009; Yue et al., 2011; Kerminen et al., 2012) which influences the radiative atmospheric  
69 forcing (Penner et al., 2011). A high particle count, such as that caused by nucleation events, has  
70 been shown to precede haze events in environments such as Beijing (Guo et al., 2014). These events  
71 are detrimental to health and quality of life. The sub-100 nm fraction of particles to which new  
72 particle formation contributes to is often referred to as the ultrafine fraction. Ultrafine particles  
73 (UFPs) pose risks to human health due to their high number concentration. UFPs exhibit gas-like  
74 behaviour and enter all parts of the lung before penetrating into the bloodstream (Miller et al.,  
75 2017). They can initiate inflammation via oxidative stress responses, progressing conditions such as

76 atherosclerosis and initiating cardiovascular responses such as hypertension through to myocardial  
77 infarction (Delfino et al., 2005; Brook et al., 2010).

78

79 Highly oxidised multifunctional molecules (HOMs), organic molecules with O:C ratios >0.6, are  
80 the result of atmospheric autoxidation and have recently been subject to much investigation, in part  
81 because the extremely low volatilities arising from their high O:C ratios favour their condensation  
82 into the particulate phase. HOMs are most well characterised as the product of oxidation of the  
83 biogenic monoterpene compound  $\alpha$ -pinene (Riccobono et al., 2014; Tröstl et al., 2016; Bianchi et  
84 al., 2017). Although globally, biogenic volatile organic compound (BVOC) concentrations far  
85 exceed ~~aromatic-anthropogenic volatile organic compound (AVOC)~~ VOC concentrations ~~by~~  
86 ~~approximately a factor of 10~~, in the urban environment the ~~aromatic-anthropogenic~~ fraction is far  
87 more significant. Formation of HOMs from aromatic compounds has been demonstrated in  
88 laboratory studies and these have been hypothesised to be large drivers of NPF in urban  
89 environments (Wang et al., 2017; Molteni et al., 2018; Qi et al., 2018). The formation of HOMs  
90 through autoxidation processes begins with the reaction of VOCs with OH, O<sub>3</sub> or NO<sub>3</sub>; formation  
91 of a peroxy radical (RO<sub>2</sub>) is followed by rapid O<sub>2</sub> additions and intra-molecular hydrogen  
92 abstractions (Jokinen et al., 2014; Rissanen et al., 2014; Kurtén et al., 2015). Furthermore,  
93 generation of oligomers from stabilised Criegee intermediates arising from short chain alkenes has  
94 been hypothesised as a contributor of Extremely Low Volatility Organic Compounds (ELVOCs)  
95 and Low Volatility Organic Compounds (LVOCs) (Zhao et al., 2015). The low volatilities of these  
96 molecules arise from their numerous oxygen-containing functionalities, and this allows them to  
97 make a significant contribution to early stage particle growth where other species cannot due to the  
98 Kelvin effect (Tröstl et al., 2016), although the contribution of HOMs to the initial molecular  
99 clusters is still debated (Kurtén et al., 2016; Elm et al., 2017; Myllys et al., 2017). ~~The result of the~~  
100 ~~large size and numerous oxygen-containing functionalities in all of these compounds is a low~~  
101 ~~vapour pressure, and therefore they make a significant contribution to particle growth (Tröstl et al.,~~

102 ~~2016), although the contribution of HOMs to the initial molecular clusters is still debated (Kurtén et~~  
103 ~~al., 2016; Elm et al., 2017; Myllys et al., 2017).~~

104

105 Recent technological advances have facilitated insights into the very first steps of nucleation which  
106 were previously unseen, with mass spectrometric techniques such as the Atmospheric Pressure  
107 Interface Time of Flight Mass Spectrometer (APi-ToF) and its chemical ionisation counterpart (CI-  
108 APi-ToF) allowing for high mass and time resolution measurements of low volatility compounds  
109 and molecular clusters. Diethylene glycol based particle counters, such as the Particle Size  
110 Magnifier (PSM) allow for measurements of particle size distributions down to the smallest  
111 molecular clusters nearing 1 nm. Recent chamber studies have elucidated the contribution of  
112 individual species to particle nucleation, ammonia and amines greatly enhancing the rate of sulfuric  
113 acid nucleation (Kirkby et al., 2011; Almeida et al., 2013). In these studies, HOMs have been  
114 identified, formed through autoxidation mechanisms (Schobesberger et al., 2013; Riccobono et al.,  
115 2014; Ehn et al., 2014). These are key to early particle growth (Tröstl et al., 2016) and can nucleate  
116 even in the absence of sulfuric acid in chambers (Kirkby et al., 2016) and in the free troposphere  
117 (Rose et al., 2018). In this paper, we report the results of HOM and particle size measurements  
118 during a summer campaign in Beijing, China.

119

## 120 **2. DATA AND METHODS**

### 121 **2.1. Sampling Site**

122 Sampling was performed as part of the [Air Pollution and Human Health in a Developing Megacity \(](#)

123 [APHH-Beijing](#)) campaign, a large international collaborative project examining emissions,  
124 processes and health effects of air pollution. For a comprehensive overview of the programme, see  
125 Shi et al. (2019). All sampling was conducted across a one month period at the Institute for  
126 Atmospheric Physics (IAP), Chinese Academy of Sciences, Beijing (39°58.53'N, 116°22.69'E).  
127 The sampling was conducted from a shipping container, with sampling inlets 1-2 metres above

128 ground level, the nearest road being 30 metres away. Meteorological parameters (wind speed, wind  
129 direction, relative humidity (RH) and temperature) were measured at the IAP meteorological tower,  
130 20 metres away from the sampling site, 30 metres from the nearest road at a height of 120 metres.  
131 Data was continuously taken from the CI-APi-ToF during a two week period, but due to data losses  
132 only five days of data is presented here. Particle size distribution measurements were taken during a  
133 33 day period from 24/05/2017 – 26/06/2017.

134

## 135 **2.2 Chemical Ionisation Atmospheric Pressure Interface Time of Flight Mass** 136 **Spectrometry**

137 The Aerodyne Nitrate Chemical Ionisation Atmospheric Pressure Interface Time of Flight Mass  
138 Spectrometer (CI-APi-ToF) was used to make measurements of neutral oxidised organic  
139 compounds, sulfuric acid and their molecular clusters at high time resolution with high resolving  
140 power. The ionization system charges molecules by adduct formation, such as in the case of organic  
141 compounds with two or more hydrogen bond donor groups (Hytinen et al., 2015), or proton  
142 transfer in the case of strong acids like sulfuric acid. Hydroxyl or hydroperoxyl functionalities are  
143 both common hydrogen bond donating groups, with hydroperoxyl being the more efficient  
144 hydrogen bond donor (Møller et al., 2017). charges molecules either by forming an adduct with  
145 NO<sub>3</sub><sup>-</sup>, or by proton transfer to NO<sub>3</sub><sup>-</sup>. The former occurs largely with species with two hydrogen bond  
146 donor groups, such as organics with two or more hydroxyl or hydroperoxyl functionalities  
147 (Hytinen et al., 2015), with hydroperoxyl being the more efficient hydrogen bond donor (Møller et  
148 al., 2017). Proton transfer occurs with molecules with great proton affinity such as sulfuric acid,  
149 although clustering with sulfuric acid does occur. This instrument has been explained in great detail  
150 elsewhere (Junninen et al., 2010; Jokinen et al., 2012), but briefly the front end consists of a  
151 chemical ionisation system where a 10 ~~Lpm~~ LPM sample flow is drawn in through the 1 metre  
152 length 1” OD stainless steel tubing opening. A secondary flow is ran was run parallel and concentric  
153 to this sample flow, rendering the reaction chamber effectively wall-less. A 3 ~~seem~~ SCCM flow of a

154 carrier gas (N<sub>2</sub>) is ~~ran~~passed over a reservoir of liquid HNO<sub>3</sub>, entraining vapour which is  
155 subsequently ionised to NO<sub>3</sub><sup>-</sup> via an X-ray source. This flow is then guided into the sample flow.  
156 containing nitrate ions generated by the X ray ionisation of nitric acid vapour is run parallel and  
157 concentric to the sample flow in an ion reaction tube. The nitrate ions will then charge molecules  
158 either by clustering or proton transfer. The mixed flows travelling at 10 ~~sLm~~ LPM enter the critical  
159 orifice at the front end of the instrument at 0.8 ~~sLm~~ LPM and are guided through a series of  
160 differentially pumped chambers before reaching the ToF analyser. Two of these chambers contain  
161 quadrupoles which can be used to select greater sensitivity for certain mass ranges, and the voltages  
162 across each individual chamber can be tuned to maximise sensitivity and resolution for ions of  
163 interest. Mass spectra are taken at a frequency of 20 kHz but are recorded at a rate of 1 Hz. All data  
164 analysis was carried out in the *Tofware* package in *Igor Pro 6* (Tofwerk AG, Switzerland). A seven  
165 point mass calibration was performed for every minute of data, and all data was normalised to  
166 signal at 62, 80 and 125 *m/Q* to account for fluctuations in ion signal, these masses representing  
167 NO<sub>3</sub><sup>-</sup>, H<sub>2</sub>ONO<sub>3</sub><sup>-</sup> and HNO<sub>3</sub>NO<sub>3</sub><sup>-</sup> respectively. The resultant normalised counts have been multiplied  
168 by 10<sup>5</sup> so magnitudes are similar to the original count rates. Typical values for calibration  
169 coefficients range from 10<sup>9</sup>-10<sup>10</sup> molecules cm<sup>-3</sup> from these normalised data (~~or 10<sup>4</sup>-10<sup>5</sup> including~~  
170 ~~the multiplication~~Kürten et al., 2012), producing peak sulfuric acid concentrations in the range of  
171 10<sup>6</sup> molecules cm<sup>-3</sup>. From the very limited periods with simultaneous data for SO<sub>2</sub>, OH radical and  
172 condensation sink, it was possible to calculate H<sub>2</sub>SO<sub>4</sub> concentrations of 10<sup>3</sup> to 10<sup>5</sup> molec cm<sup>-3</sup>, in  
173 which range the calibration constant was 7.0 ± 1.6 x 10<sup>8</sup> cm<sup>-3</sup> which fits well with that expected for  
174 this concentration range (Kürten et al., 2012). The nitrate-water cluster is included as the presence  
175 of many nitrate-water clusters of the general formula (H<sub>2</sub>O)<sub>x</sub>(HNO<sub>3</sub>)<sub>y</sub>NO<sub>3</sub><sup>-</sup> were found, where *x* =  
176 (1, 2, 3... 20) and *y* = (0, 1). No sensitivity calibration was performed for these measurements, and  
177 so all values are reported in signal intensity, ions/s normalised signal intensity. Due to the high  
178 resolving power of the CI-APi-ToF system (mass resolution of 3500 *m/dm* and mass accuracy of 20  
179 ppm at 288 *m/Q*), multiple peaks can be fit at the same unit mass and their molecular formulae

180 assigned. These peaks follow the general formula  $C_xH_yO_zN_w$  where  $x = 2-20$ ,  $y = 2-32$ ,  $z = 4-16$   
181 and  $w = 0-2$ , spanning from small organic acids like oxalic and malonic acid through to large  
182 dimers of oxidised monoterpene  $RO_2$  radicals such as  $C_{20}H_{31}O_9N$ . Beyond  $500 m/Q$ , peak fitting  
183 and assignment of compositions becomes problematic as signal decreases, mass accuracy decreases,  
184 and the total number of chemical compositions increases, so peaks above the  $C_{20}$  region have not  
185 been assigned, and a number of peaks have been unassigned due to this uncertainty (Cubison and  
186 Jimenez, 2015). As proton transfer mostly happens with acids, and nearly all HOM molecules will  
187 be charged by adduct formation it is possible to infer the uncharged formula; therefore all HOMs  
188 from here onwards will be listed as their uncharged form.

189

### 190 **2.3. Size Distribution Measurements**

191 Two Scanning Mobility Particle Sizer (SMPS) instruments measured particle size distributions at  
192 15 minute time resolution, one LongSMPS (TSI 3080 EC, 3082 Long DMA, 3775 CPC, TSI, USA)  
193 and one NanoSMPS (3082 EC, 3082 Nano DMA, 3776 CPC, TSI, USA) measuring the ranges ~~4-65~~  
194 14-615 nm and ~~4-65~~ 14-615-nm respectively. A Particle Size Magnifier (A10, Airmodus, FN)  
195 linked to a CPC (3775, TSI, USA) measured the sub-3 nm size fraction. The PSM was run in  
196 stepping mode, operating at four different saturator ~~pressures-flows~~ to vary the lowest size cut-off of  
197 particles that it will grow (this cut-off is technically a point of 50% detection efficiency) of <1.30,  
198 1.36, 1.67 and 2.01 nm. The instrument switched between saturator ~~pressures-flows~~ per 2.5 minutes,  
199 giving a sub-2.01 nm size distribution every 10 minutes. The data was treated with a moving  
200 average filter to account for jumps in total particle count, and due to the similar behaviour of the  
201 two upper and two lower size cuts, these have been averaged to two size cuts at 1.30 and 1.84 nm.

202

### 203 **2.4. Calculations**

204 The condensation sink (CS) was calculated from the size distribution data as follows:

$$(1)$$

$$CS = 4\pi D \sum_{d'_p} \beta_{m,d'_p} d'_p N_{d'_p}$$

205  
206  
207  
208  
209  
210

where D is the diffusion coefficient of the diffusing vapour (assumed sulfuric acid), ~~and~~  $\beta_m$  is a transition regime correction (Kulmala et al., 2012),  $d'_p$  is particle diameter, and  $N_{d'_p}$  is the number of particles at diameter  $d'_p$ .

## 211 2.5. Other Measurements

212 Measurements of the classical air pollutants were measured on the same site, and have been  
213 reported in the campaign overview paper (Shi et al., 2019). SO<sub>2</sub> was measured using a 43i SO<sub>2</sub>  
214 analyser (ThermoFisher Scientific, USA), O<sub>3</sub> with a 49i O<sub>3</sub> analyser (ThermoFisher Scientific,  
215 USA) and NO<sub>x</sub> with a 42i-TL Trace NO<sub>x</sub> analyser (ThermoFisher Scientific, USA), and a T500U  
216 CAPS NO<sub>2</sub> analyser (~~Enviro Technology Services~~ Teledyne API, USA). VOC mixing ratios were  
217 measured using a Proton Transfer Reaction-Time of Flight-Mass Spectrometer (PTR-ToF 2000,  
218 Ionicon, Austria).

219

## 220 3. RESULTS AND DISCUSSION

### 221 3.1. Characteristics of Sampling Period

222 A total of five days of CI-API-ToF data were collected successfully, from 2017/06/21 midday  
223 through 2017/06/26 midday. New particle formation events were observed on 24<sup>th</sup> June in the late  
224 afternoon and 25<sup>th</sup> June at midday. Some nighttime formation of molecular clusters was seen  
225 earlier in the campaign, as were several peaks to the 1.5 – 100 nm size range, likely from pollutant  
226 plumes containing freshly nucleating condensable materials. The trace gases, O<sub>3</sub>, SO<sub>2</sub>, NO and NO<sub>2</sub>  
227 are plotted in the Figure S1. O<sub>3</sub> shows mid-afternoon peaks, around ~120 ppb<sub>v</sub> on the first two days  
228 of the campaign, and 50-70 ppb<sub>v</sub> for the latter days. SO<sub>2</sub> shows a large peak, reaching 4 ppb<sub>v</sub> on  
229 22/06 but <1 ppb<sub>v</sub> for the rest of campaign. NO shows strong mid-morning rush hour related peaks,



230 declining towards midday due to being rapidly consumed by O<sub>3</sub>. NO<sub>2</sub> shows large traffic related  
231 peaks. The sulfuric acid signal across this period as measured by NO<sub>3</sub><sup>-</sup> CI-API-ToF showed strong  
232 midday peaks, with concentrations-signal highest on 24/06/2017 and 25/06/2017. The  
233 meteorological data are shown in Figure S2 alongside condensation sink (CS). The conditions were  
234 generally warm and humid, with temperature reaching its maximum on 25/06/2017, with a peak  
235 hourly temperature of 31°C. High temperatures were seen on 21/06 and 24/06 also, of 30°C and  
236 26°C respectively.

237

## 238 **3.2. Gas Phase HOM Chemistry**

### 239 **3.2.1. Bulk chemical properties**

240 For the peaks that ~~that~~ have had chemical formulae assigned, oxidation state of carbon, or  $OS_c$ , can  
241 be used to describe their bulk oxidation chemistry.  $OS_c$  is defined as (Kroll et al., 2011)

242

$$243 \quad OS_c = (2 \times O:C) - H:C \quad (2)$$

244

245 This does not account for the presence of nitrate ester groups, which has been accounted for  
246 previously by subtracting five times the N:C ratio (Massoli et al., 2018), under the assumption that  
247 all nitrogen containing functionality is in the form of nitrate ester (RONO<sub>2</sub>) groups. In Beijing,  
248 multiple sources of nitrate-containing organic compounds are seen, in the forms of amines, nitriles  
249 and heterocycles. The variation of oxidation state with carbon number ( $C_n$ ) without correction for  
250 nitrate esters is plotted in Figure 1. The average oxidation state of carbon in this dataset tends to  
251 decrease with an increase to  $C_n$ , highest where  $C_n = 5$ , attributable both to high O:C and peak area  
252 for the peak assigned to C<sub>5</sub>H<sub>10</sub>N<sub>2</sub>O<sub>8</sub> at  $m/Q$  288.  $C_n = 5$  also shows the greatest distribution of  
253 oxidation states, likely due to the high ambient concentration of isoprene and therefore its many  
254 oxidation products being of high enough concentrations-signal for many well resolved peaks to be  
255 seen in this dataset. It is worth notinge that some of the ions plotted here may not form through

256 peroxy radical autoxidation, such as C<sub>5</sub>H<sub>10</sub>N<sub>2</sub>O<sub>8</sub>, which may be a second-generation oxidation  
257 product of isoprene under high NO<sub>x</sub> (Lee et al., 2016). -C<sub>n</sub>=10 and 15 also see a small increase to  
258 average oxidation number compared to their neighbours. The lower oxidation state of the larger  
259 products is likely a function of two things. First and foremost, any autoxidation mechanism must  
260 undergo more steps in order for a larger molecule to reach an equivalent O:C ratio with a smaller  
261 one, and the equivalent O:C ratio is ultimately less likely to be reached before the radical is  
262 terminated (Massoli et al., 2018). Secondly, the lower vapour pressures of these larger products will  
263 lead to their partitioning into the condensed phase more readily than the smaller, thus they are more  
264 rapidly lost (Mutzel et al., 2015).

265  
266 The degrees of OS<sub>c</sub> observed here are similar to those seen in other environments such as during  
267 the SOAS campaign in 2013 in southern United States, characterised by low NO/NO<sub>2</sub> and high  
268 temperatures, where campaign averages of 0.3 ppb, 0.4-0.5 ppb, and 25°C respectively were  
269 measured, although an additional parameter to account for nitrogen containing VOCs is included in  
270 the calculation (Massoli et al., 2018). The OS<sub>c</sub> observed in Beijing is also higher than that seen in  
271 the boreal forest environment of Hyytiälä, despite extremely low NO<sub>x</sub> concentrations, likely due to  
272 low temperature conditions dominating in those conditions (Schobesberger et al., 2013). These  
273 relatively similar degrees of oxidation to those seen in other, cleaner, environments are likely due to  
274 an interplay between the higher temperatures facilitating rapid hydrogen abstractions (Crouse et  
275 al., 2013; Praske et al., 2018; Quéléver et al., 2018) and the higher concentrations of NO<sub>x</sub>, HO<sub>2</sub>, and  
276 other RO<sub>2</sub> molecules terminating the autoxidation sequence more efficiently (Praske et al., 2018,  
277 Rissanen, 2018, Garmash et al., 2019).

278  
279 A mass defect plot is shown in Figure 2, which shows nominal mass plotted against mass defect for  
280 all peaks in this dataset. Kendrick mMass defect can be defined as the Kendrick ion mass -minus  
281 Kendrick-integer mass. This is shown for two separate daytime periods, one where nucleation was

282 not occurring and HOM concentrations are lower (10:30 – 12:00 23/06/2017) and one where  
283 nucleation was occurring under high HOM concentrations (10:30 – 12:00 25/06/2017).- The band of  
284 lower mass defect is characterised by a number of large peaks with high signal, ~~for example, at  $m/Q$~~   
285 ~~344 the ion  $(\text{NH}_3)_3(\text{H}_2\text{SO}_4)_2\text{HSO}_4^-$  and  $(\text{H}_2\text{O})_2(\text{NH}_3)_2(\text{H}_2\text{SO}_4)_2\text{HSO}_4^-$  at  $m/Q$  362., for example, at~~  
286  $m/Q$  436 the ion  $(\text{C}_2\text{H}_7\text{N})_2(\text{H}_2\text{SO}_4)_2\text{HSO}_4^-$ . Many water clusters are seen here. ~~This clustering may~~  
287 ~~happen in the atmosphere, in the chemical ionisation inlet or through the critical orifice in the small~~  
288 ~~segmented quadrupole (SSQ) section of the instrument, and there is a weak dependence of these~~  
289 ~~concentrations on the SSQ pressure.~~ The upper component of the mass defect is dominated by  
290 organic compoundss, the upper end of more positive mass defect is occupied by molecules with  
291 more  $^1\text{H}$  (mass defect 7.825 mDa) and  $^{14}\text{N}$  (mass defect 3.074 mDa). The end of less positive mass  
292 defect has lower  $^1\text{H}$  and more  $^{16}\text{O}$  (mass defect -5.085 mDa); alternatively put, the mass defect  
293 reflects the variation in  $OS_c$ . The organic components with more positive mass defects will be more  
294 volatile than their lower mass defect counterparts as they will contain fewer oxygen functionalities  
295 (Tröstl et al., 2016, Stolzenburg et al., 2018). These higher volatility products may still contribute to  
296 larger size particle growth. The more negative mass defect components will be those of greater O:C  
297 and therefore lower volatility, LVOCs, and the yet larger and more oxidised components, ELVOCs  
298 (Tröstl et al., 2016). During the nucleation period, the signal intensity for the species in the upper  
299 band of more negative mass defect have the most marked increase in concentration, with  
300 significantly less difference  $>500 m/Q$ . This region 200-400  $m/Q$  will contain most of the  $\text{C}_5+$   
301 monomer HOMs seen in this dataset.

302

### 303 3.2.2. Diurnal trends of HOMs

304 Temporal trends of HOMs in the urban atmosphere can ~~throw light upon~~reveal their sources and  
305 behaviour in the atmosphere. Most of the HOM species peak in the daytime. These species all  
306 follow a similar diurnal trend, as shown in Figure 3. Both the concentrations of  $\text{O}_3$  and  $\text{OH}$  are high  
307 during ~~this period~~ the summer period in Beijing (although the nitrate chemical ionisation technique

308 is not sensitive to all OH oxidation products (Berndt et al., 2015)). Figure S1 shows the time series  
309 of concentrations of NO which is considered a dominant peroxy radical terminator of particular  
310 importance in the polluted urban environment (Khan et al., 2015). ~~Peroxy radicals~~Radicals such as  
311 HO<sub>2</sub><sup>·</sup> and RO<sub>2</sub><sup>·</sup> also typically peak during daytime. The HOM components peaking in the daytime  
312 are presumed to be the oxidation products of a mixture of anthropogenic and biogenic components,  
313 such as alkylbenzenes, monoterpenes and isoprene. The oxidation of monoterpenes, specifically the  
314 monoterpene  $\alpha$ -pinene, has been the subject of extensive study recently, with the O<sub>3</sub>-initiated  
315 autoxidation sequence being the best characterised (Ehn et al., 2014; Jokinen et al., 2014; Kurtén et  
316 al., 2015; Kirkby et al., 2016); ozonolysis of  $\alpha$ -pinene opens the ring structure and produces a RO<sub>2</sub><sup>·</sup>  
317 radical (Kirkby et al., 2016). In the case of aromatics, OH addition to the ring and the subsequently  
318 formed bicyclic peroxy radical is the basis for the autoxidation of compounds such as xylenes and  
319 trimethylbenzenes (Molteni et al., 2018; Wu et al., 2017).

320

321 The identified compounds have been roughly separated into several categories, each of these plotted  
322 in Figure 3. ~~Figure 3a~~The top of this graph shows the separation of components into ~~HOM and ON~~  
323 ~~(organonitrate)~~ non-nitrogen containing HOMs, and nitrogen containing HOMs, or organonitrates  
324 (ONs) components. The ON signal is much higher than that of the HOM, attributable in part to a  
325 few ions of high signal, such as the isoprene organonitrate C<sub>5</sub>H<sub>10</sub>N<sub>2</sub>O<sub>8</sub>. A few similar structural  
326 formulae are seen (C<sub>5</sub>H<sub>10</sub>N<sub>2</sub>O<sub>6</sub>, C<sub>5</sub>H<sub>11</sub>NO<sub>6</sub>, C<sub>5</sub>H<sub>11</sub>NO<sub>7</sub>, etc), some of which have been identified as  
327 important gas phase oxidation products of isoprene under high NO<sub>x</sub> conditions (Xiong et al., 2015),  
328 and their contribution to SOA has been explored previously (Lee et al., 2016). A high nitrophenol  
329 signal is also seen, C<sub>6</sub>H<sub>5</sub>NO<sub>3</sub>. The signal for HOM compounds is less dominated by a few large  
330 ions. The prevalence of ON compounds points towards the important role of NO<sub>x</sub> as a peroxy  
331 radical terminator, with the probability for the RO<sub>2</sub><sup>·</sup> + NO<sub>x</sub> reaction to produce nitrate ester  
332 compounds increasing with the size of the RO<sub>2</sub><sup>·</sup> molecule (Atkinson et al., 1982). The NO<sub>x</sub>  
333 concentrations in urban Beijing are approximately a factor of 10 higher than seen at the Hyytiälä

334 station in Finland as reported by Yan et al. (2016), and hence it is expected to be a more significant  
335 peroxy radical terminator.

336

337 Despite the very large fluxes of anthropogenic organic pollutants in Beijing, biogenic emissions are  
338 still an important source of reactive VOCs in the city, with abundant isoprene oxidation products  
339 observed (see above), as well as monoterpene monomers ( $C_{10}H_{16}O_9$ ,  $C_{10}H_{15}O_9N$ ) and some dimer  
340 products ( $C_{20}H_{30}O_{11}$ ,  $C_{20}H_{31}O_{11}N$ ). The time series of the ~~concentrations~~ signals of all  $C_5$ ,  $C_{10}$  and  
341  $C_{20}$  molecules is plotted in ~~the middle panel of~~ Figure 3b, with  $C_5$  species assumed to be isoprene  
342 dominated,  $C_{10}$  and  $C_{20}$  assumed to be monoterpene dominated. Signals for ~~isoprene~~ isoprene oxidation  
343 products are ~~present at~~ higher ~~concentrations~~, with abundant isoprene nitrate and dinitrate products.  
344  $C_{10}$  products show similar behaviour, with, for example, several  $C_{10}H_{15}O_xN$   $x = 5-9$  compounds  
345 seen. The  $C_{20}$  signal intensities are low ~~products seen are low in concentration~~, and follow the  
346 general formula  $C_{20}H_xO_yN_z$ , where  $x = 26-32$ ,  $y = 7-11$  and  $z = 0-2$ ; in Figure 3 the signal for  $C_{20}$   
347 compounds has been multiplied by a factor of 50 for visibility. The low ~~concentrations~~ signals  
348 reflect the lack of  $RO_2$  cross reactions necessary for the production of these accretion products.

349

350 Other identified peaks are plotted in ~~the bottom panel of~~ Figure 3c. The  $C_2$ - $C_4$  components are  
351 summed together, these being small organic acids such as malonic acid and oxalic acid, as well as  
352 products such as  $C_4H_7O_6N$ . Malonic acid is the most prominent here, seen both as an  $NO_3^-$  adduct  
353 ( $C_3H_4O_4NO_3^-$ ) and a proton transfer product ( $C_3H_3O_4^-$ ) at a ratio of around 2:3. The  $C_6$ - $C_9$   
354 components are assumed to be dominated by oxidation products of alkylbenzenes such as  $C_8H_{12}O_5$ ,  
355 although fragments of other compounds, i.e., monoterpenes, can also occupy this region (Isaacman-  
356 Vanwertz et al., 2018). It is assumed the majority of the signal for these peaks come from  
357 alkylbenzenes. This assumption is supported by the relative signal intensity ratios of the oxygen  
358 numbers of monomer  $C_8H_{12}O_n$  compounds being similar to those seen for xylene oxidation products  
359 in previous work (Molteni et al., 2018). The largest fraction,  $C_{11}$  through  $C_{18}$ , includes the larger

360 compounds, oxidation products of larger aromatics, or products of the cross reaction of smaller RO<sub>2</sub>  
361 radicals. Here they are grouped without more sophisticated disaggregation as they all follow much  
362 the same time series, species such as C<sub>11</sub>H<sub>11</sub>O<sub>8</sub>N following the same temporal trends as C<sub>15</sub>H<sub>16</sub>O<sub>9</sub>  
363 and C<sub>16</sub>H<sub>24</sub>O<sub>12</sub>.

364

365 Nearly all ions with the exception of the larger compounds attributed to the cross reaction of C<sub>10</sub>  
366 monomers follow similar temporal patterns, with the majority of peaks occurring in the daytime.

367 This reflects the importance of the concentration of atmospheric oxidants. Some selected oxidation  
368 products are plotted against their precursor VOCs in Figure 4. The concentration of isoprene is

369 plotted against the ~~concentration~~ signal of a nitrate HOM product, C<sub>5</sub>H<sub>9</sub>NO<sub>6</sub> (Xiong et al., 2015;

370 Lee et al., 2016), while monoterpenes are plotted against C<sub>10</sub>H<sub>16</sub>O<sub>9</sub> (Ehn et al., 2014; Berndt et al.,

371 2016; Yan et al., 2016; Kirkby et al., 2016; Massoli et al., 2018), and C<sub>2</sub>-benzenes against C<sub>8</sub>H<sub>12</sub>O<sub>6</sub>

372 (Molteni et al., 2018; Wang et al., 2017). The first half of the time series shows little correlation

373 between the VOC species and the resultant oxidation products, while isoprene, monoterpenes and

374 C<sub>2</sub>-benzenes follow their usual diurnal cycles, isoprene having the most distinct with a strong

375 midday peak. The latter two days, however, show similar and coinciding peaks in both the VOCs

376 and HOMs - HOMs show afternoon peaks on both days, and an initial shelf on the final half day.

377 The C<sub>5</sub>H<sub>9</sub>NO<sub>6</sub> peak follows some of the peaks of the isoprene, but not all (e.g., morning shelf of

378 isoprene on 24/06). Concentrations of isoprene do not seem to determine directly the ~~concentration~~

379 signal of HOM, as the day with the lowest isoprene of all is the day with highest C<sub>5</sub>H<sub>9</sub>NO<sub>6</sub>. The

380 C<sub>10</sub>H<sub>16</sub>O<sub>9</sub> trace has coincidental peaks with the monoterpene trace also, including two 4-hour

381 separated simultaneous peaks on 25/06. The peaks in the concentrations of C<sub>2</sub>-benzenes are nearly

382 synchronous with the peaks in C<sub>8</sub>H<sub>12</sub>O<sub>6</sub>, ~~for which the peaksdata; these~~ exhibit a strong mid early

383 afternoon peak likely due to the lack of an efficient ozonolysis reaction pathway; the main oxidant

384 of C<sub>2</sub>-benzenes is the OH radical. Trends of both C<sub>3</sub> benzenes and their HOMs are much the same

385 as C<sub>2</sub> benzenes as discussed above, pointing to similar sources and oxidation chemistries. This

386 ~~behaviour is much the same as the C<sub>3</sub>-benzenes and their oxidation products.~~ The concentration of  
387 precursor VOC is likely a driving force in the identity and quantity of various HOM products, but  
388 not the sole determinant, as while there are simultaneous peaks of VOCs and HOMs, both the  
389 condensation sink and oxidant concentrations also influence HOM product ~~concentrations~~signals.

391 The first half of campaign measurements is marked by an episode of low HOM  
392 ~~concentrations~~signals. A diurnal cycle still exists but it is weak. The radiation intensity was  
393 significantly lower on these prior days than it was on the 24th. No data is available for the final  
394 period of measurement. Ozone is higher on the prior measurement days with lower HOM  
395 ~~concentrations~~signals (see Figure [S2S1](#)). It is therefore plausible that light intensity, and therefore  
396 OH concentration is one of the main drivers of HOM concentrations in Beijing.

397  
398 The C<sub>20</sub> compounds [plotted in Figure 3b](#) show no strong diurnal sequence, contrasting with other  
399 HOMs. We can presume that all C<sub>20</sub> compounds identified are the result of the reaction of two  
400 monoterpene C<sub>10</sub> RO<sub>2</sub> radicals, a reasonable assumption as all identified C<sub>20</sub> species follow the  
401 general formula outlined for these reactions (C<sub>20</sub>H<sub>28-32</sub>O<sub>6-16</sub>). The formation of C<sub>20</sub> dimers is  
402 dependent upon two processes, initial oxidation of monoterpenes, and RO<sub>2</sub>-RO<sub>2</sub> termination. Initial  
403 oxidation is contingent upon oxidant concentration, which is highest in the daytime, and RO<sub>2</sub>-RO<sub>2</sub>  
404 termination is contingent upon the probability of the molecular collision between the RO<sub>2</sub>  
405 molecules occurring before other radical termination (i.e., RO<sub>2</sub>-NO<sub>x</sub>, or RO<sub>2</sub>-HO<sub>2</sub>). There is likely  
406 a strong diurnal sequence in the dominant RO<sub>2</sub> termination mechanisms across the day period, and  
407 the combination of the two factors discussed above results in there being no strong diurnal trend in  
408 these molecules. A lower oxidant concentration at night results in less RO<sub>2</sub> molecules, but less NO  
409 and HO<sub>2</sub> results in a greater chance for those RO<sub>2</sub> molecules to ~~dimerize~~dimerise ([Rissanen, 2018](#),  
410 [Garmash et al., 2019](#)). As the levels of NO<sub>x</sub> in Beijing fall, the peroxy radical termination reactions  
411 will be less probable compared to continued autoxidation ([Praske et al., 2018](#)), and it is expected

412 that more oxidised HOM products will be seen with lower volatilities and therefore a greater  
413 potential contribution to earlier stage particle formation and growth.

### 414 3.3. New Particle Formation

415 Nearly all the signal intensity in the CI-APi-ToF instrument arises from molecules charged by  $\text{NO}_3^-$ ,  
416 therefore plotting the unit mass resolution data (the data gained by integrating over the entire area at  
417 each m/Q integer) data against time describes simply the evolution of oxidised organic molecules,  
418 acids and their molecular clusters both with each other and stabilising amine species. This is done in  
419 Figure 5. As the signal intensity varies by factors of 10 from mass to mass, all each value masses  
420 have has been normalised ~~to 1~~ so they have maxima at 1. This has been done separately for two days  
421 for clarity, as the signal intensity also varies from day to day. PSM data for these two days is plotted  
422 in Figure 5 also, with both total particle count  $>1.30$  nm in black and the number difference  
423 between the lower and upper size cuts (1.30 and 1.84 nm) in blue, which shows the number of  
424 particles between these sizes. The relationship between mass and electrical mobility diameter can be  
425 defined thus (Tammets, 1995),

426

$$427 \quad d_e = \left(\frac{6m}{\pi\rho}\right)^{\frac{1}{3}} + d_g \quad (3)$$

428

429 where  $d_e$  is the electrical mobility diameter of the cluster or particle,  $m$  is the mass of the cluster or  
430 particle expressed in kg,  $\rho$  is the density and  $d_g$  is the effective gas diameter, determined to be 0.3  
431 nm for smaller particles (Larriba et al., 2011). We can use this to draw a comparison between the  
432 PSM and CI-APi-ToF measurements. If a density of  $1.2 \text{ g cm}^{-3}$  is assumed, then once molecular  
433 clusters reach the  $>400 \text{ m/Q}$  range, they will be seen in the lowest size cut of the PSM, or  $>700 \text{ m/Q}$   
434 if a density of  $2.0 \text{ g cm}^{-3}$  is assumed. A full table of densities is provided in the Supplementary  
435 Information.

436



437 A burst in the signal seen by the CI-APi-TOF occurs first in the late morning in the top panel of  
438 Figure 5, and this is at the same time as peaks begin to rise in the identified HOMs (see Figure 3).  
439 Here, the PSM is not available due to an instrumental fault until 16:00; however, at that point, an  
440 elevation to particle count and a large elevation to cluster count can be seen. Moving into the  
441 evening period, the mass contour shows peaks to larger masses  $>400 m/Q$ . This is likely ~~dimerized~~  
442 ~~dimerised~~ compounds and ~~products of~~  $\text{NO}_3^-$  chemistry with little contribution to newly forming  
443 particles, but still sensitive to chemical ionisation by  $\text{NO}_3^-$ . Many of these peaks cannot be assigned  
444 due to uncertainties in the structural formula assignment for higher mass peaks, as the number of  
445 possible dimerised compounds is many, being the combination of most possible  $\text{RO}_2$  radicals.  
446 Graphically, these are over-represented in Figure 5 due to the normalisation, their ~~concentrations~~  
447 ~~signals~~ (especially  $>500 m/Q$ ) are much lower than the ~~concentrations-signals~~  $<400 m/Q$ .

448  
449 The second day plotted in the lower panel of Figure 5 (25/06/2017) shows a strong afternoon peak  
450 to the HOMs (for most HOMs, stronger than that on the day prior). Particle formation is shown in  
451 the PSM data. A strong midday peak to particle number is seen with two distinct peaks to cluster  
452 count. These two peaks are not coincidental with the two peaks to HOM ~~concentrations-signal~~ (i.e.,  
453 ~~nitrogen-containing HOMs in Figure 3a peaking at 11:00 and 16:00~~) ~~nor the two peaks in aromatic~~  
454 ~~VOCs (i.e.,  $\text{C}_2$ -benzenes in Figure 4)~~. Sulfuric acid, however, does peak synchronously with the  
455 particle number count. Sulfuric acid is plotted across the contour plot in Figure 6, where PSM data  
456 is also shown in the bottom panel. The peak to CI-APi-TOF mass ~~signal~~, visible in Figure 5 occurs  
457 at around 12:00/13:00, peaks in the PSM cluster count occur at 10:00 and 13:00. ~~Peaks in mass up~~  
458 ~~to 550  $m/Q$  are seen in the CI-APi-ToF at 13:00. Assuming the density of these species is  $\leq 1.6 \text{ g cm}^{-3}$~~   
459 ~~then these will be suitably sized to be grown in the PSM saturator. — at 13:00 the peaks in mass~~  
460 ~~occur between 200-550  $m/Q$ . Assuming the density of the identified species is  $\leq 1.6 \text{ g cm}^{-3}$  then~~  
461 ~~these will be suitably sized to be grown in the PSM saturator above the size cut at 1.30 nm. The~~  
462 ~~peak at 10:00 in PSM cluster count is characterised by a few peaks at specific masses (around 680,~~

463 ~~720, 840, 860  $m/Q$ ), presumably specific nucleating inorganic clusters, pointing towards a possible~~  
464 ~~evolution in the composition of clusters throughout the nucleation event with the early nucleation~~  
465 ~~linked with a few specific precursors.~~ These newly formed particles then go on to grow and  
466 contribute significantly to the larger particle count (Figure S3). As initial particle formation  
467 coincides with sulfuric acid ~~concentrations~~ signal peaks and before HOM ~~concentrations~~ signals  
468 peak, it can be assumed on these days, the HOM contribution to the initial particle formation is  
469 modest.

470

471 There is recent strong evidence to suggest that the driving force of the earliest stages of particle  
472 formation in urban Shanghai is from sulfuric acid and C<sub>2</sub>-amines (Yao et al., 2018), ~~supported~~  
473 ~~by~~ and the coincidental peaks of sulfuric acid with new particles as seen in Figure 6 suggest a  
474 similar behaviour. Dimethylamine (DMA) can efficiently stabilise the sulfuric acid clusters  
475 (Almeida et al., 2013). Here, few larger sulfuric acid-DMA clusters were visible in the dataset, as  
476 seen in the work by Yao et al., 2018, although five sulfuric acid-dimethylamine (SA-DMA) ions  
477 were observed, the others were likely too low in signal to be confidently resolved from their  
478 neighbouring peaks; however, clusters of up to 4 sulfuric acid ions and 3 dimethylamine molecules  
479 were seen, with similar diurnal trends to sulfuric acid. The scarcity of ~~SA~~ sulfuric acid-DMA  
480 clusters is likely due to instrumental conditions, rather than their absence in the atmosphere. The  
481 nitrate chemical ionisation system tends to evaporate amine compounds upon charging, and as  
482 specific voltage-tuning setups can lend themselves towards preservation or breakage of molecular  
483 clusters, the signal for larger sulfuric acid clusters was also very weak. The formation of HOM-  
484 sulfuric acid clusters is unlikely under atmospheric conditions (Elm et al., 2017) and few of these  
485 were observed. ~~Concentrations~~ Signals of HOMs seem to coincide with later particle growth; it can  
486 be expected that HOM molecules make a more significant contribution to particle growth than to  
487 early particle formation, with the largest and most oxidised being involved in early growth, and the

488 smaller and less oxidised contributing to later growth as the necessary vapour pressure properties  
489 become less demanding.

490

491

#### 492 **4. CONCLUSIONS**

493 The average degree of HOM oxidation in Beijing is comparable with that seen in other  
494 environments. Rapid intramolecular hydrogen shifts during autoxidation due to the higher  
495 temperatures are probably offset by the frequent termination reactions due to high NO<sub>x</sub>  
496 concentrations. OS<sub>c</sub> values seem to be marginally higher for biogenic species.

497

498 The temporal trend of nearly every HOM shows afternoon or evening ~~daytime~~ maxima. Both O<sub>3</sub>  
499 and OH have high daytime concentrations and these likely drive the initial oxidation steps. The  
500 species arising from alkylbenzene precursors show sharper afternoon peaks, probably since their  
501 oxidation is OH dominated. Many of the rest of the peaks, coming from largely BVOC precursors  
502 show broader daytime peaks, being influenced by O<sub>3</sub> also. There seems to be no direct link between  
503 VOC concentrations and HOM concentrationssignals, with days of lower precursor VOC  
504 sometimes having higher HOM concentrations-signals and vice versa.

505

506 Initial particle formation coincides with peak sulfuric acid concentrationssignals, while the growth  
507 of the particles correlates more closely with the concentrations-signals of HOMs. This is very  
508 similar to behaviour observed in a study of NPF in Shanghai which was attributed to sulfuric acid-  
509 dimethylamine-water nucleation with condensing organic species contributing to particle growth  
510 (Yao et al., 2018), and this is further backed up by numerous SA-DMA clusters present in this  
511 dataset. The freshly formed particles grow and contribute significantly to total particle loading.  
512 This is visible when the unit mass CI-APi-ToF data is plotted as a contour plot, and further to this is  
513 visible in the PSM data, with bursts to both total number count >1.30 nm and the number of

514 molecular clusters between 1.30 and 1.84 nm. As NO<sub>x</sub> levels fall in Beijing due to traffic emission  
515 control measures being enforced it is likely that autoxidation will become increasingly significant in  
516 the new particle formation processes. The number of molecules detected by the NO<sub>3</sub> CIMS is  
517 undoubtedly many more than have had formulae assigned here, but to identify more requires a more  
518 sophisticated data deconvolution.

519

## 520 **DATA ACCESSIBILITY**

521 Data supporting this publication are openly available from the UBIRA eData repository at  
522 <https://doi.org/10.25500/edata.bham.00000304>

523

## 524 **AUTHOR CONTRIBUTIONS**

525 The study was conceived and planned by RMH and ZS. DCSB and JB set up and operated the  
526 main instrumental measurements, and JB prepared the first draft of the paper and responded to  
527 comments from RMH and ZS. CNH and WJA contributed the hydrocarbon data and provided  
528 comments on the draft manuscript, and ES and JL contributed the gas phase pollutant data.

529

## 530 **COMPETING INTERESTS**

531 The authors have no conflict of interests.

532

## 533 **ACKNOWLEDGMENTS**

534 This work was part of the APHH-Beijing programme funded by the UK Natural Environment  
535 Research Council (NE/N007190/1) and the Natural Sciences Funding Council of China. It was  
536 additionally facilitated by the National Centre for Atmospheric Science ODA national capability  
537 programme ACREW (NE/R000034/1), which is supported by NERC and the GCRF. We thank  
538 Professor X.M Wang from the Guangzhou Institute of Geochemistry, Chinese Academy of  
539 Sciences, Brian Davison from Lancaster University and Ben Langford, Eiko Nemitz, Neil

540 Mullinger and other staff from the Centre for Ecology and Hydrology, Edinburgh for assistance  
541 with the VOC measurements and associated infrastructure.

542

543 **REFERENCES**

544

545 Alam, A., Shi, J.P., Harrison R.M.: Observations of new particle formation in urban air, *J. Geophys.*  
546 *Res.*, 108, 4093-4107, doi:10.1029/2001JD001417, 2003

547

548 Almeida, J., Schobesberger, S., Kürten, A., Ortega, I. K., Kupiainen-Määttä, O., Praplan, A. P.,  
549 Adamov, A., Amorim, A., Bianchi, F., Breitenlechner, M., David, A., Dommen, J., Donahue, N.  
550 M., Downard, A., Dunne, E., Duplissy, J., Ehrhart, S., Flagan, R. C., Franchin, A., Guida, R.,  
551 Hakala, J., Hansel, A., Heinritzi, M., Henschel, H., Jokinen, T., Junninen, H., Kajos, M.,  
552 Kangasluoma, J., Keskinen, H., Kupc, A., Kurtén, T., Kvashin, A. N., Laaksonen, A., Lehtipalo, K.,  
553 Leiminger, M., Leppä, J., Loukonen, V., Makhmutov, V., Mathot, S., McGrath, M. J., Nieminen,  
554 T., Olenius, T., Onnela, A., Petäjä, T., Riccobono, F., Riipinen, I., Rissanen, M., Rondo, L.,  
555 Ruuskanen, T., Santos, F. D., Sarnela, N., Schallhart, S., Schnitzhofer, R., Seinfeld, J. H., Simon,  
556 M., Sipilä, M., Stozhkov, Y., Stratmann, F., Tomé, A., Tröstl, J., Tsagkogeorgas, G., Vaattovaara,  
557 P., Viisanen, Y., Virtanen, A., Vrtala, A., Wagner, P. E., Weingartner, E., Wex, H., Williamson, C.,  
558 Wimmer, D., Ye, P., Yli-Juuti, T., Carslaw, K. S., Kulmala, M., Curtius, J., Baltensperger, U.,  
559 Worsnop, D. R., Vehkamäki, H., and Kirkby, J.: Molecular understanding of sulphuric acid-amine  
560 particle nucleation in the atmosphere, *Nature*, 502, 359-363, 2013.

561

562 Atkinson, R., Aschmann, S. M., Carter, W. P. L., Winer, A. M., and Pitts, J. N.: Alkyl nitrate  
563 formation from the nitrogen oxide (NO<sub>x</sub>)air photooxidations of C2-C8 n-alkanes, *J. Phys. Chem.*,  
564 86, 4563-4569, 1982.

565

566 Berndt, T., Richters, S., Kaethner, R., Voigtländer, J., Stratmann, F., Sipilä, M., Kulmala, M., and  
567 Herrmann, H.: Gas-Phase Ozonolysis of Cycloalkenes: Formation of Highly Oxidized RO2  
568 Radicals and Their Reactions with NO, NO2, SO2, and Other RO2 Radicals, *J. Phys. Chem. A.*,  
569 119, 10336-10348, 2015.

570

571 Berndt, T., Richters, S., Jokinen, T., Hyttinen, N., Kurtén, T., Otkjær, R. V., Kjaergaard, H. G.,  
572 Stratmann, F., Herrmann, H., Sipilä, M., Kulmala, M., and Ehn, M.: Hydroxyl radical-induced  
573 formation of highly oxidized organic compounds, *Nature Comm.*, 7, 20  
574 <https://doi.org/10.1038/ncomms13677>, 2016.

575

576 Bianchi, F., Garmash, O., He, X., Yan, C., Iyer, S., Rosendahl, I., Xu, Z., Rissanen, M. P., Riva, M.,  
577 Taipale, R., Sarnela, N., Petäjä, T., Worsnop, D. R., Kulmala, M., Ehn, M., and Junninen, H.: The  
578 role of highly oxygenated molecules (HOMs) in determining the composition of ambient ions in the  
579 boreal forest, *Atmos. Chem. Phys.*, 17, 13819-13831, 2017.

580

581 Brook, R. D., Rajagopalan, S., Pope, C. A., Brook, J. R., Bhatnagar, A., Diez-Roux, A. V., Holguin,  
582 F., Hong, Y., Luepker, R. V., Mittleman, M. A., Peters, A., Siscovick, D., Smith, S. C., Whitsel, L.,  
583 and Kaufman, J. D.: Particulate matter air pollution and cardiovascular disease: An update to the  
584 scientific statement from the american heart association, *Circulation*, 121, 2331-2378, 2010.

585

586 Chu, B., Kerminen, V.-M., Bianchi, F., Yan, C., Petaja, T., and Kulmala, M.: Atmospheric new  
587 particle formation in China, *Atmos. Chem. Phys.*, 19, 115-138, 2019.

588

589 Crouse, J. D., Nielsen, L. B., Jørgensen, S., Kjaergaard, H. G., and Wennberg, P. O.: Autoxidation  
590 of organic compounds in the atmosphere, *J. Phys. Chem. Lett.*, 4, 3513-3520, 2013.

591

592

593

594 Cubison, M. J. and Jimenez, J. L.: Statistical precision of the intensities retrieved from constrained  
595 fitting of overlapping peaks in high resolution mass spectra, *Atmos. Meas. Tech.*, 8, 2333-2345,  
596 2015.

597

598 Delfino, R. J., Sioutas, C., and Malik, S.: Potential role of ultrafine particles in associations between  
599 airborne particle mass and cardiovascular health, *Environ. Health Perspect.*, 113, 934-946, 2005.

600

601 Ehn, M., Thornton, J. A., Kleist, E., Sipilä, M., Junninen, H., Pullinen, I., Springer, M., Rubach, F.,  
602 Tillmann, R., Lee, B., Lopez-Hilfiker, F., Andres, S., Acir, I.-H., Rissanen, M., Jokinen, T.,  
603 Schobesberger, S., Kangasluoma, J., Kontkanen, J., Nieminen, T., Kurtén, T., Nielsen,  
604 L. B., Jørgensen, S., Kjaergaard, H. G., Canagaratna, M., Maso, M. D., Berndt, T., Petäjä, T.,  
605 Wahner, A., Kerminen, V.-M., Kulmala, M., Worsnop, D. R., Wildt, J., and Mentel, T. F.: A large  
606 source of low-volatility secondary organic aerosol, *Nature*, 506, 476-479, 2014.

607

608 Elm, J., Myllys, N., and Kurtén, T.: What is Required for Highly Oxidized Molecules to Form  
609 Clusters with Sulfuric Acid?, *J. Phys. Chem. A*, 121, 4578-4587, 2017.

610

611 Garmash, O., Rissanen, M. P., Pullinen, I., Schmitt, S., Kausiala, O., Tillmann, R., Percival, C.,  
612 Bannan, T. J., Priestley, M., Hallquist, Å. M., Kleist, E., Kiendler-Scharr, A., Hallquist, M., Berndt,  
613 T., McFiggans, G., Wildt, J., Mentel, T., and Ehn, M.: Multi-generation OH oxidation as a source  
614 for highly oxygenated organic molecules from aromatics, *Atmos. Chem. Phys. Discuss.*,  
615 <https://doi.org/10.5194/acp-2019-582>, in review, 2019.

616

617 Gong, Y., Hu, M., Cheng, Y., Su, H., Yue, D., Liu, F., Wiedensohler, A., Wang, Z., Kalesse, H.,  
618 Liu, S., Wu, Z., Xiao, K., Mi, P., and Zhang, Y.: Competition of coagulation sink and source rate:  
619 New particle formation in the Pearl River Delta of China, *Atmos. Environ.*, 44, 3278-3285, 2010.

620

621 Guo, S., Hu, M., Zamora, M. L., Peng, J., Shang, D., Zheng, J., Du, Z., Wu, Z., Shao, M., Zeng, L.,  
622 Molina, M. J., and Zhang, R.: Elucidating severe urban haze formation in China., *PNAS*, 111,  
623 17373- 17378, 2014.

624

625 Hyttinen, N., Kupiainen-Määttä, O., Rissanen, M. P., Muuronen, M., Ehn, M., and Kurtén, T.:  
626 Modeling the Charging of Highly Oxidized Cyclohexene Ozonolysis Products Using Nitrate-Based  
627 Chemical Ionization, *J. Phys. Chem., A*, 119, 6339-6345, 2015.

628

629 Isaacman-Vanwertz, G., Massoli, P., O'Brien, R., Lim, C., Franklin, J. P., Moss, J. A., Hunter, J. F.,  
630 Nowak, J. B., Canagaratna, M. R., Misztal, P. K., Arata, C., Roscioli, J. R., Herndon, S. T., Onasch,  
631 T. B., Lambe, A. T., Jayne, J. T., Su, L., Knopf, D. A., Goldstein, A. H., Worsnop, D. R., and Kroll,  
632 J. H.: Chemical evolution of atmospheric organic carbon over multiple generations of oxidation,  
633 *Nature Chem.*, 10, 462-468, <https://doi.org/10.1038/s41557-018-0002-2>, 2018

634

635 Jokinen, T., Sipilä, M., Junninen, H., Ehn, M., Lönn, G., Hakala, J., Petäjä, T., Mauldin, R. L.,  
636 Kulmala, M., and Worsnop, D. R.: Atmospheric sulphuric acid and neutral cluster measurements  
637 using CI-APi-TOF, *Atmos. Chem. Phys.*, 12, 4117-4125, 2012.

638

639 Jokinen, T., Sipilä, M., Richters, S., Kerminen, V. M., Paasonen, P., Stratmann, F., Worsnop, D.,  
640 Kulmala, M., Ehn, M., Herrmann, H., and Berndt, T.: Rapid autoxidation forms highly oxidized  
641 RO<sub>2</sub> radicals in the atmosphere, *Angewandte Chemie - International Edition*, 53, 14596-14600,  
642 <https://doi.org/10.1002/anie.201408566>, 2014.

643

644

645 Junninen, H., Ehn, M., Petäjä, Luosujärvi, L., Kotiaho, T., Kostianen, R., Rohner, U., Gonin, M.,  
646 Fuhrer, K., Kulmala, M., and Worsnop, D. R.: A high-resolution mass spectrometer to measure  
647 atmospheric ion composition, *Atmos. Meas. Tech.*, 3, 1039-1053, 2010.  
648

649 Kerminen, V. M., Paramonov, M., Anttila, T., Riipinen, I., Fountoukis, C., Korhonen, H., Asmi, E.,  
650 Laakso, L., Lihavainen, H., Swietlicki, E., Svenningsson, B., Asmi, A., Pandis, S. N., Kulmala, M.,  
651 and Petäjä, T.: Cloud condensation nuclei production associated with atmospheric nucleation: A  
652 synthesis based on existing literature and new results, *Atmos. Chem. Phys.*, 12, 12037-12059, 2012.  
653

654 Khan, M., Cooke M, Utembe, S., Archibald A., Derwent, R., Jenkin, M., Morris, W., South, N.,  
655 Hansen, J., Francisco, J., Percival, C., Shallcross, D.: Global analysis of peroxy radicals and peroxy  
656 radical-water complexation using the STOCHEM-CRI global chemistry and transport model,  
657 *Atmos. Environ.*, 106, 278-287, 2015.  
658

659 Kirkby, J., Curtius, J., Almeida, J., Dunne, E., Duplissy, J., Ehrhart, S., Franchin, A., Gagné, S.,  
660 Ickes, L., Kürten, A., Kupc, A., Metzger, A., Riccobono, F., Rondo, L., Schobesberger, S.,  
661 Tsagkogeorgas, G., Wimmer, D., Amorim, A., Bianchi, F., Breitenlechner, M., David, A.,  
662 Dommen, J., Downard, A., Ehn, M., Flagan, R. C., Haider, S., Hansel, A., Hauser, D., Jud, W.,  
663 Junninen, H., Kreissl, F., Kvashin, A., Laaksonen, A., Lehtipalo, K., Lima, J., Lovejoy, E. R.,  
664 Makhmutov, V., Mathot, S., Mikkilä, J., Minginette, P., Mogo, S., Nieminen, T., Onnela, A.,  
665 Pereira, P., Petäjä, T., Schnitzhofer, R., Seinfeld, J. H., Sipilä, M., Stozhkov, Y., Stratmann, F.,  
666 Tomé, A., Vanhanen, J., Viisanen, Y., Vrtala, A., Wagner, P. E., Walther, H., Weingartner, E.,  
667 Wex, H., Winkler, P. M., Carslaw, K. S., Worsnop, D. R., Baltensperger, U., and Kulmala, M.:  
668 Role of sulphuric acid, ammonia and galactic cosmic rays in atmospheric aerosol nucleation,  
669 *Nature*, 476, 429-435, <https://doi.org/10.1038/nature10343>, 2011.  
670

671 Kirkby, J., Duplissy, J., Sengupta, K., Frege, C., Gordon, H., Williamson, C., Heinritzi, M., Simon,  
672 M., Yan, C., Almeida, J., Trostl, J., Nieminen, T., Ortega, I. K., Wagner, R., Adamov, A., Amorim,  
673 A., Bernhammer, A. K., Bianchi, F., Breitenlechner, M., Brilke, S., Chen, X., Craven, J., Dias, A.,  
674 Ehrhart, S., Flagan, R. C., Franchin, A., Fuchs, C., Guida, R., Hakala, J., Hoyle, C. R., Jokinen, T.,  
675 Junninen, H., Kangasluoma, J., Kim, J., Krapf, M., Kurten, A., Laaksonen, A., Lehtipalo, K.,  
676 Makhmutov, V., Mathot, S., Molteni, U., Onnela, A., Perakyla, O., Piel, F., Petaja, T., Praplan, A.  
677 P., Pringle, K., Rap, A., Richards, N. A., Riipinen, I., Rissanen, M. P., Rondo, L., Sarnela, N.,  
678 Schobesberger, S., Scott, C. E., Seinfeld, J. H., Sipilä, M., Steiner, G., Stozhkov, Y., Stratmann, F.,  
679 Tomé, A., Virtanen, A., Vogel, A. L., Wagner, A. C., Wagner, P. E., Weingartner, E., Wimmer, D.,  
680 Winkler, P. M., Ye, P., Zhang, X., Hansel, A., Dommen, J., Donahue, N. M., Worsnop, D. R.,  
681 Baltensperger, U., Kulmala, M., Carslaw, K. S., and Curtius, J.: Ion-induced nucleation of pure  
682 biogenic particles, *Nature*, 533, 521-526, <https://doi.org/10.1038/nature17953>, 2016.  
683

684 Kroll, J. H., Donahue, N. M., Jimenez, J. L., Kessler, S. H., Canagaratna, M. R., Wilson, K. R.,  
685 Altieri, K. E., Mazzoleni, L. R., Wozniak, A. S., Bluhm, H., Mysak, E. R., Smith, J. D., Kolb, C. E.,  
686 and Worsnop, D. R.: Carbon oxidation state as a metric for describing the chemistry of atmospheric  
687 organic aerosol, *Nature Chemistry*, 3, 133-139, <https://doi.org/10.1038/nchem.948>, 2011.  
688

689 Kulmala, M., Petäjä, T., Mönkkönen, P., Koponen, I. K., Dal Maso, M., Aalto, P. P., Lehtinen, K.  
690 E. J., and Kerminen, V.-M.: On the growth of nucleation mode particles: source rates of  
691 condensable vapor in polluted and clean environments, *Atmos. Chem. Phys.*, 5, 409-416, 2005.  
692

693 Kulmala, M., Petäjä, T., Nieminen, T., Sipilä, M., Manninen, H. E., Lehtipalo, K., Dal Maso, M.,  
694 Aalto, P. P., Junninen, H., Paasonen, P., Riipinen, I., Lehtinen, K. E. J., Laaksonen, A., and  
695 Kerminen, V.-M.: Measurement of the nucleation of atmospheric aerosol particles, *Nature*  
696 *Protocols*, 7, 1651-1667, <https://doi.org/10.1038/nprot.2012.091>, 2012.



697 Kürten, A., Rondo, L., Ehrhart, S., and Curtius, J.: Caibration of a chemical ionization mass  
698 spectrometer for the measurement of gaseous sulfuric acid, J. Phys. Chem., A, 116, 6375-6386.  
699

700 Kurtén, T., Rissanen, M. P., Mackeprang, K., Thornton, J. A., Hyttinen, N., Jørgensen, S., Ehn, M.,  
701 and Kjaergaard, H. G.: Computational Study of Hydrogen Shifts and Ring-Opening Mechanisms in  
702  $\alpha$ -Pinene Ozonolysis Products, J. Phys. Chem., A, 119, 11366-11375, 2015.  
703

704 Kurtén, T., Tiusanen, K., Roldin, P., Rissanen, M., Luy, J. N., Boy, M., Ehn, M., and Donahue, N.:  
705  $\alpha$ -Pinene autoxidation products may not have extremely low saturation vapor pressures despite high  
706 O:C ratios, J. Phys. Chem., A, 120, 2569-2582, 2016.  
707

708 Larriba, C., Hogan, C. J., Attoui, M., Borrajo, R., Garcia, J. F., and De La Mora, J. F.: The  
709 mobility-volume relationship below 3.0 nm examined by tandem mobility-mass measurement,  
710 Aerosol Sci. Techn., 45, 453-467, 2011.  
711

712 Lee, B. H., Mohr, C., Lopez-Hilfiker, F. D., Lutz, A., Hallquist, M., Lee, L., Romer, P., Cohen, R.  
713 C., Iyer, S., Kurtén, T., Hu, W., Day, D. A., Campuzano-Jost, P., Jimenez, J. L., Xu, L., Ng, N. L.,  
714 Guo, H., Weber, R. J., Wild, R. J., Brown, S. S., Koss, A., de Gouw, J., Olson, K., Goldstein, A. H.,  
715 Seco, R., Kim, S., McAvey, K., Shepson, P. B., Starn, T., Baumann, K., Edgerton, E. S., Liu, J.,  
716 Shilling, J. E., Miller, D. O., Brune, W., Schobesberger, S., D'Ambro, E. L., and Thornton, J. A.:  
717 Highly functionalized organic nitrates in the southeast United States: Contribution to secondary  
718 organic aerosol and reactive nitrogen budgets, PNAS, 113, 1516-1521, 2016.  
719

720 Lehtipalo, K., Yan, C., Dada, L., Bianchi, F., Xiao, M., Wagner, R., Stolzenburg, D., Ahonen, L. R.,  
721 Amorim, A., Baccarini, A., Bauer, P. S., Baumgartner, B., Bergen, A., Bernhammer, A.,  
722 K., Breitenlechner, M., Brilke, S., Buchholz, A., Mazon, S. B., Chen, D., Chen, X., Dias, A.,  
723 Dommen, J., Draper, D. C., Duplissy, J., Ehn, M., Finkenzeller, H., Fischer, L., Frege, C., Fuchs,  
724 C., Garmash, O., Gordon, H., Hakala, J., He, X., Heikkinen, L., Heinritzi, M., Helm, J. C., Hofbauer,  
725 V., Hoyle, C. R., Joki-nen, T., Kangasluoma, J., Kerminen, V.-M., Kim, C., Kirkby, J., Kontkanen,  
726 J., Kürten, A., Lawler, M. J., Mai, H., Mathot, S., Mauldin, R. L., Molteni, U., Nichman, L., Nie,  
727 W., Niemi-nen, T., Ojdanic, A., Onnela, A., Passananti, M., Petäjä, T., Piel, F., Pospisilova, V.,  
728 Quéléver, L. L. J., Rissanen, M. P., Rose, C., Sarnela, N., Schallhart, S., Schuchmann, S., Sengupta,  
729 K., Simon, M., Sipilä, M., Tauber, C., Tomé, A., Tröstl, J., Väisänen, O., Vogel, A. L., Volkamer,  
730 R., Wagner, A. C., Wang, M., Weitz, L., Wimmer, D., Ye, P., Ylisirniö, A., Zha, Q., Carslaw, K. S.,  
731 Curtius, J., Donahue, N. M., Flagan, R. C., Hansel, A., Riipinen, I., Virtanen, A., Winkler, P. M.,  
732 Baltensperger, U., Kulmala, M., and Worsnop, D. R.: Multicomponent new particle formation from  
733 sulfuric acid, ammonia, and biogenic vapors, Science Advances, 4,  
734 <https://doi.org/10.1126/sciadv.aau5363>, 2018.  
735

736 Massoli, P., Stark, H., Canagaratna, M. R., Krechmer, J. E., Xu, L., Ng, N. L., Mauldin, R. L., Yan,  
737 C., Kimmel, J., Misztal, P. K., Jimenez, J. L., Jayne, J. T., and Worsnop, D. R.: Ambient  
738 Measurements of Highly Oxidized Gas-Phase Molecules during the Southern Oxidant and Aerosol  
739 Study (SOAS) 2013, ACS Earth Space Chem., 2, 653-672, 2018.  
740

741 McMurry, P. H., Shan Woo, K., Weber, R., Chen, D.-R., and Pui, D. Y. H.: Size distributions of 3-  
742 10 nm atmospheric particles: implications for nucleation mechanisms, Philosophical Transactions  
743 of the Royal Society A: Math., Phys. Eng. Sci., 358, 2625-2642, 2000.  
744

745 Miller, M. R., Raftis, J. B., Langrish, J. P., McLean, S. G., Samueltai, P., Connell, S. P., Wilson, S.,  
746 Vesey, A. T., Fokkens, P. H., Boere, A. J. F., Krystek, P., Campbell, C. J., Hadoke, P. W.,  
747 Donaldson, K., Cassee, F. R., Newby, D. E., Duffin, R., and Mills, N. L.: Inhaled nanoparticles  
748 accumulate at sites of vascular disease, ACS Nano, 11, 4542-4552, 2017.

749 Møller, K. H., Tram, C. M., and Kjaergaard, H. G.: Side-by-Side Comparison of Hydroperoxide  
750 and Corresponding Alcohol as HydrogenBond Donors, *J. Phys. Chem. A*, 121, 2951-2959, 2017.  
751

752 Molteni, U., Bianchi, F., Klein, F., Haddad, I. E., Frege, C., Rossi, M. J., Dommen, J., and  
753 Baltensperger, U.: Formation of highly oxygenated organic molecules from aromatic compounds,  
754 *Atmos. Chem. Phys.*, 18, 1909-1921, 2018.  
755

756 Mutzel, A., Poulain, L., Berndt, T., Iinuma, Y., Rodigast, M., Böge, O., Richters, S., Spindler, G.,  
757 Sipila, M., Jokinen, T., Kulmala, M., Herrmann, H.: Highly oxidized multifunctional organic  
758 compounds observed in tropospheric particles: A field and laboratory study, *Environ. Sci. Technol.*,  
759 49, 7754-7761, 2015.  
760

761 Myllys, N., Olenius, T., Kurtén, T., Vehkamäki, H., Riipinen, I., and Elm, J.: Effect of Bisulfate,  
762 Ammonia, and Ammonium on the Clustering of Organic Acids and Sulfuric Acid, *J. Phys. Chem.*  
763 *A*, 121, 4812-4824, 2017.  
764

765 Penner, J. E., Xu, L., and Wang, M.: Satellite methods underestimate indirect climate forcing by  
766 aerosols., *PNAS*, 108, 13404-13408, 2011.  
767

768 Praske, E., Otkjær, R. V., Crounse, J. D., Hethcox, J. C., Stoltz, B. M., Kjaergaard, H. G., and  
769 Wennberg, P. O.: Atmospheric autoxidation is increasingly important in urban and suburban North  
770 America, *PNAS*, 115, 64-69, 2018.  
771

772 Qi, X., Ding, A., Roldin, P., Xu, Z., Zhou, P., Sarnela, N., Nie, W., Huang, X., Rusanen, A., Ehn,  
773 M., Rissanen, M. P., Petäjä, T., Kulmala, M., and Boy, M.: Modelling studies of HOMs and their  
774 contributions to new particle formation and growth: comparison of boreal forest in Finland and a  
775 polluted environment in China, *Atmos. Chem. Phys.*, 18, 11779-11791, 2018.  
776

777 Quéléver, J., Kristensen, K., Normann Jensen, L., Teiwes, R., Daellenbach, Kaspar R., Peräkylä, O.,  
778 Roldin, P., Pedersen, H., Glasius, M., Bilde, M., Ehn, M.: Effect of temperature on the formation of  
779 Highly-oxygenated Organic Molecules (HOM) from alpha-pinene ozonolysis, *Atmos. Chem. Phys.*  
780 *Discuss.*, 18, 1-29, 2018.  
781

782 Riccobono, F., Schobesberger, S., Scott, C., Dommen, J., Ortega, I., Rondo, L., Almeida, J.,  
783 Amorim, A., Bianchi, F., Breitenlechner, M., David, A., Downard, A., Dunne, E., Duplissy, J.,  
784 Ehrhart, S., Flagan, R., Franchin, A., Hansel, A., Junninen, H., Kajos, M., Keskinen, H., Kupc, A.,  
785 Kürten, A., Kvashin, A., Laaksonen, A., Lehtipalo, K., Makhmutov, V., Mathot, S., Nieminen, T.,  
786 Onnela, A., Petäjä, T., Praplan, A., Santos, F., Schallhart, S., Seinfeld, J., Sipilä, M., Van Spracklen,  
787 D., Stozhkov, Y., Stratmann, F., Tomé, A., Tsagkogeorgas, G., Vaattovaara, P., Viisanen, Y.,  
788 Vrtala, A., Wagner, P., Weingartner, E., Wex, H., Wimmer, D., Carslaw, K., Curtius, J., Donahue,  
789 N., Kirkby, J., Kulmala, M., Worsnop, D., and Baltensperger, U.: Oxidation products of biogenic  
790 emissions contribute to nucleation of atmospheric particles, *Science*, 344, 717-721, 2014.  
791

792 Rissanen, M. P., Kurtén, T., Sipilä, M., Thornton, J. A., Kangasluoma, J., Sarnela, N., Junninen, H.,  
793 Jørgensen, S., Schallhart, S., Kajos, M. K., Taipale, R., Springer, M., Mentel, T. F., Ruuskanen, T.,  
794 Petäjä, T., Worsnop, D. R., Kjaergaard, H. G., and Ehn, M.: The formation of highly oxidized  
795 multifunctional products in the ozonolysis of cyclohexene, *J. Am. Chem. Soc.*, 136, 15596-15606  
796 2014.  
797

798 [Rissanen, M. P.: NO<sub>2</sub> Suppression of Autoxidation–Inhibition of Gas-Phase Highly Oxidized Dimer](#)  
799 [Product Formation, \*ACS Earth Space Chem.\*, 2, 1211–1219,](#)  
800 <https://doi.org/10.1021/acsearthspacechem.8b00123>, 2018.

801 Rose, C., Zha, Q., Dada, L., Yan, C., Lehtipalo, K., Junninen, H., Mazon, S. B., Jokinen, T.,  
802 Sarnela, N., Sipilä, M., Petäjä, T., Kerminen, V.-M., Bianchi, F., and Kulmala, M.: Observations of  
803 biogenic ion-induced cluster formation in the atmosphere, *Sci. Adv.*, 4, eaar5218,  
804 <https://doi.org/10.1126/sciadv.aar5218>, 2018.

805  
806 Schobesberger, S., Junninen, H., Bianchi, F., Lönn, G., Ehn, M., Lehtipalo, K., Dommen, J.,  
807 Ehrhart, S., Ortega, I. K., Franchin, A., Nieminen, T., Riccobono, F., Hutterli, M., Duplissy, J.,  
808 Almeida, J., Amorim, A., Breitenlechner, M., Downard, A. J., Dunne, E. M., Flagan, R. C., Kajos,  
809 M., Keskinen, H., Kirkby, J., Kupc, A., Kürten, A., Kurtén, T., Laaksonen, A., Mathot, S., Onnela,  
810 A., Praplan, A. P., Rondo, L., Santos, F. D., Schallhart, S., Schnitzhofer, R., Sipilä, M., Tomé, A.,  
811 Tsagkogeorgas, G., Vehkamäki, H., Wimmer, D., Baltensperger, U., Carslaw, K. S., Curtius, J.,  
812 Hansel, A., Petäjä, T., Kulmala, M., Donahue, N. M., and Worsnop, D. R.: Molecular  
813 understanding of atmospheric particle formation from sulfuric acid and large oxidized organic  
814 molecules., *PNAS*, 110, 17223-17228, 2013.

815  
816 Shi, J. P., Evans, D. E., Khan, A. A., and Harrison, R. M.: Sources and concentration of  
817 nanoparticles (<10nm diameter) in the urban atmosphere, *Atmos. Environ.*, 35, 1193-1202, 2001.

818  
819 Shi, Z., Vu, T., Kotthaus, S., Harrison, R.M., Grimmond, S., Yue, S., Zhu, T., Lee, J., Han, Y.,  
820 Demuzere, M., Dunmore, R.E., Ren, L., Liu, D., Wang, Y., Wild, O., Allan, J., Acton, W.J.,  
821 Barlow, J., Barratt, B., Beddows, D., Bloss, W.J., Calzolari, G., Carruthers, D., Carslaw, D.C., Chan,  
822 Q., Chatzidiakou, L., Chen, Y., Crilley, L., Coe, H., Dai, T., Doherty, R., Duan, F., Fu, P., Ge, B.,  
823 Ge, M., Guan, D., Hamilton, J.F., He, K., Heal, M., Heard, D., Hewitt, C.N., Hollaway, M., Hu, M.,  
824 Ji, X. Jiang, R. Jones, M. Kalberer, F.J. Kelly, L. Kramer, B. Langford, C. Lin, A.C. Lewis, J. Li,  
825 W. Li, D., Liu, H., Liu, J., Loh, M., Lu, K., Lucarelli, F., Mann, G., McFiggans, G., Miller, M.R.,  
826 Mills, G., Monk, P., Nemitz, E., O'Connor, F., Ouyang, B., Palmer, P.I., Percival, C., Popoola, O.,  
827 Reeves, C., Rickard, A.R., Shao, L., Shi, G., Spracklen, D., Stevenson, D., Sun, Y., Sun, Z., Tao, S.,  
828 Tong, S., Wang, Q., Wang, W., Wang, X., Wang, X., Wang, Z., Wei, L., Whalley, L., Wu, X., Wu,  
829 Z., Xie, P., Yang, F., Zhang, Q., Zhang, Y., Zhang, Y. and Zheng, M.: In-depth study of air  
830 pollution sources and processes within Beijing and its surrounding region (APHH-Beijing), *Atmos.*  
831 *Chem. Phys.*, 19, 7519-7546, 2019.

832  
833 Stolzenburg, D, Fischer, L., Vogel, A., Heinritzi, M., Schervish, M., Simon, M., Wagner, A.,  
834 Dada, L., Ahonen, L., Amorim, A., Baccharini, A., Bauer, P., Baumgartner, B., Bergen, A.,  
835 Bianchi, F., Breitenlechner, M., Brilke, S., Buenrostro Mazon, S., Chen, D., Dias, A., Draper, D.,  
836 Duplissy, J., El Haddad, I., Finkenzeller, H., Frege, C., Fuchs, C., Garmash, O., Gordon, H., He, X.,  
837 Helm, J., Hofbauer, V., Hoyle, C., Kim, C., Kirkby, J., Kontkanen, J., Kürten, A., Lampilahti, J.,  
838 Lawler, M., Lehtipalo, K., Leiminger, M., Mai, H., Mathot, S., Mentler, B., Molteni, U., Nie, W.,  
839 Nieminen, T., Nowak, J., Ojdanic, A., Onnela, A., Passananti, M., Petäjä, T., Quéléver, L.,  
840 Rissanen, M., Sarnela, N., Schallhart, S., Tauber, C., Tomé, A., Wagner, R., Wang, M., Weitz, L.,  
841 Wimmer, D., Xiao, M., Yan, C., Ye, P., Zha, Q., Baltensperger, U., Curtius, J., Dommen, J., Flagan,  
842 R., Kulmala, M., Smith, J., Worsnop, D., Hansel, A., Donahue, N., Winkler, P., Rapid growth of  
843 organic aerosol nanoparticles over a wide tropospheric temperature range, *PNAS*, 115, 9122-9127,  
844 2018.

845  
846 Tammet, H.: Size and mobility of nanometer particles, clusters and ions, *J. Aerosol Sci.*, 26, 459-  
847 475, 1995.

848  
849 Tomasi, C., Fuzzi, S., Kokhanovsky, A.: *Atmospheric Aerosols: Life Cycles and Effects on Air*  
850 *Quality and Climate*, Wiley, 2016.

851

852 Tröstl, J., Chuang, W. K., Gordon, H., Heinritzi, M., Yan, C., Molteni, U., Ahlm, L., Frege, C.,  
853 Bianchi, F., Wagner, R., Simon, M., Lehtipalo, K., Williamson, C., Craven, J. S., Duplissy, J.,  
854 Adamov, A., Almeida, J., Bernhammer, A. K., Breitenlechner, M., Brilke, S., Dias, A., Ehrhart, S.,  
855 Flagan, R. C., Franchin, A., Fuchs, C., Guida, R., Gysel, M., Hansel, A., Hoyle, C. R., Jokinen, T.,  
856 Junninen, H., Kangasluoma, J., Keskinen, H., Kim, J., Krapf, M., Kürten, A., Laaksonen, A.,  
857 Lawler, M., Leiminger, M., Mathot, S., Möhler, O., Nieminen, T., Onnela, A., Petäjä, T., Piel, F.  
858 M., Miettinen, P., Rissanen, M. P., Rondo, L., Sarnela, N., Schobesberger, S., Sengupta, K., Sipilä,  
859 M., Smith, J. N., Steiner, G., Tomè, A., Virtanen, A., Wagner, A. C., Weingartner, E., Wimmer, D.,  
860 Winkler, P. M., Ye, P., Carslaw, K. S., Curtius, J., Dommen, J., Kirkby, J., Kulmala, M., Riipinen,  
861 I., Worsnop, D. R., Donahue, N. M., and Baltensperger, U.: The role of low-volatility organic  
862 compounds in initial particle growth in the atmosphere, *Nature*, 533, 527-531,  
863 <https://doi.org/10.1038/nature18271>, 2016.

864  
865 Wang, S., Wu, R., Berndt, T., Ehn, M., and Wang, L.: Formation of Highly Oxidized Radicals and  
866 Multifunctional Products from the Atmospheric Oxidation of Alkylbenzenes, *Environ. Sci. Techn.*,  
867 51, 8442-8449, 2017.

868  
869 Wang, Z., Wu, Z., Yue, D., Shang, D., Guo, S., Sun, J., Ding, A., Wang, L., Jiang, J., Guo, H., Gao,  
870 J., Cheung, H. C., Morawska, L., Keywood, M., and Hu, M.: New particle formation in China:  
871 Current knowledge and further directions, *Sci. Tot. Environ.*, 577, 258-266, 2016.

872  
873 Wiedensohler, A., Cheng, Y. F., Nowak, A., Wehner, B., Achtert, P., Berghof, M., Birmili, W., Wu,  
874 Z. J., Hu, M., Zhu, T., Takegawa, N., Kita, K., Kondo, Y., Lou, S. R., Hofeumahaas, A., Holland,  
875 F., Wahner, A., Gunthe, S. S., Rose, D., Su, H., and Pöschl, U.: Rapid aerosol particle growth and  
876 increase of cloud condensation nucleus activity by secondary aerosol formation and condensation:  
877 A case study for regional air pollution in northeastern China, *Journal of Geophysical Research*  
878 *Atmospheres*, 114, 1–13, <https://doi.org/10.1029/2008JD010884>, 2009.

879  
880 Wu, Z., Hu, M., Lin, P., Liu, S., Wehner, B., and Wiedensohler, A.: Particle number size  
881 distribution in the urban atmosphere of Beijing, China, *Atmos. Environ.*, 42, 7967-7980, 2008.

882  
883 Wu, Z., Ma, N., Größ, J., Kecorius, S., Lu, K., Shang, D., Wang, Y., Wu, Y., Zeng, L., Hu, M.,  
884 Wiedensohler, A., and Zhang, Y.: Thermodynamic properties of nanoparticles during new particle  
885 formation events in the atmosphere of North China Plain, *Atmos. Res.*, 188, 55-63, 2017.

886  
887 Wu, Z. J., Hu, M., Liu, S., Wehner, B., Bauer, S., Ssling, a. M., Wiedensohler, a., Petäjä, T., Dal  
888 Maso, M., and Kulmala, M.: New particle formation in Beijing, China: Statistical analysis of a 1-  
889 year data set, *J. Geophys. Res. Atmospheres*, 112, D09209, <https://doi.org/10.1029/2006JD007406>,  
890 2007.

891  
892 Xiong, F., McAvey, K. M., Pratt, K. A., Groff, C. J., Hostetler, M. A., Lipton, M. A., Starn, T. K.,  
893 Seeley, J. V., Bertman, S. B., Teng, A. P., Crouse, J. D., Nguyen, T. B., Wennberg, P. O., Misztal,  
894 P. K., Goldstein, A. H., Guenther, A. B., Koss, A. R., Olson, K. F., De Gouw, J. A., Baumann, K.,  
895 Edgerton, E. S., Feiner, P. A., Zhang, L., Miller, D. O., Brune, W. H., and Shepson, P. B.:  
896 Observation of isoprene hydroxynitrates in the Southeastern United States and implications for the  
897 fate of NO<sub>x</sub>, *Atmos. Chem. Phys.*, 15, 11257-11272, 2015 .

898  
899 Yan, C., Nie, W., Äijälä, M., Rissanen, M. P., Canagaratna, M. R., Massoli, P., Junninen, H.,  
900 Jokinen, T., Sarnela, N., Häme, S. A. K., Schobesberger, S., Canonaco, F., Yao, L., Prévôt, A. S.  
901 H., Petäjä, T., Kulmala, M., Sipilä, M., Worsnop, D. R., and Ehn, M.: Source characterization of  
902 highly oxidized multifunctional compounds in a boreal forest environment using positive matrix  
903 factorization, *Atmos. Chem. Phys.*, 16, 12715-12731, 2016.

904 Yao, L., Garmash, O., Bianchi, F., Zheng, J., Yan, C., Kontkanen, J., Junninen, H., Mazon, S. B.,  
905 Ehn, M., Paasonen, P., Sipilä, M., Wang, M., Wang, X., Xiao, S., Chen, H., Lu, Y., Zhang, B.,  
906 Wang, D., Fu, Q., Geng, F., Li, L., Wang, H., Qiao, L., Yang, X., Chen, J., Kerminen,  
907 V. M., Petäjä, T., Worsnop, D. R., Kulmala, M., and Wang, L.: Atmospheric new particle formation  
908 from sulfuric acid and amines in a Chinese megacity, *Science*, 361, 278-281, 2018.  
909  
910 Yu, F. and Luo, G.: Simulation of particle size distribution with a global aerosol model:  
911 Contribution of nucleation to aerosol and CCN number concentrations, *Atmospheric Chemistry and*  
912 *Physics*, 9, 7691-7710, 2009.  
913  
914 Yue, D. L., Hu, M., Zhang, R. Y., Wu, Z. J., Su, H., Wang, Z. B., Peng, J. F., He, L. Y., Huang, X.  
915 F., Gong, Y. G., and Wiedensohler, A.: Potential contribution of new particle formation to cloud  
916 condensation nuclei in Beijing, *Atmos. Environ.*, 45, 6070-6077, 2011.  
917  
918 Zhao, Y., Wingen, L. M., Perraud, V., Greaves, J., and Finlayson-Pitts, B. J.: Role of the reaction of  
919 stabilized Criegee intermediates with peroxy radicals in particle formation and growth in air, *Phys.*  
920 *Chem. Chem. Phys.*, 17, 12500-12514, 2015.  
921

922 **FIGURE LEGENDS:**

923

924 **Figure 1** Oxidation state of carbon calculated as two times the oxygen to carbon ratio minus the  
925 hydrogen to carbon ratio against carbon number for (colored) individual ions and (blue  
926 circles) signal weighted average for each carbon number. Area and colour are both  
927 proportional to the peak area for each ion

928

929 **Figure 2** Mass defect plot of fitted mass spectral peaks between 100-600mass units on (a) 10:30  
930 – 12:00 23/06/2017, a non nucleation day, and (b) 10:30 -12:00 25/06/2017, a  
931 nucleation day. Mass defect can be defined as the mass - integer mass. The size of point  
932 is proportional to the signal intensity. As  $^1\text{H}$  has a positive mass defect (1.007276 Da),  
933 the upward trend along the horizontal indicates increasing carbon chain length, and  
934 differences at similar masses are due to increasing oxygen functionality, clustering with  
935 species such as sulfuric acid (negative mass defect) and ammonia (positive mass  
936 defect), as  $^{16}\text{O}$  and  $^{32}\text{S}$  have negative mass defects (15.9949 and 31.9721 Da  
937 respectively), while  $^{14}\text{N}$  has a positive mass defect at 14.0031 Da.

938

939 **Figure 3** Summed time series of the concentrations of ([topA](#)) all non-nitrogen containing HOMs  
940 and all organonitrates identified, ([middleB](#)) C5, C10 and C20 components, assumed to  
941 be dominated by isoprene, monoterpene monomer and monoterpene dimers, signal for  
942 C20 multiplied 50 times to fit scale, and ([bottomC](#)) summed C6 - C9 components, and  
943 summed C11 - C18 components, assumed to be dominated by alkylbenzenes and other  
944 larger components respectively.

945

946 **Figure 4** Time series for the whole sampling campaign for the concentrations of (left axis) VOCs  
947 as measured by PTR-ToF and (right axis) a selected HOM product associated with that  
948 precursor.

949

950 **Figure 5** Normalised unit mass  $\text{NO}_3$ - CI-APi-ToF signal intensity on 24/06/2017 ([topA](#)) and  
951 25/06/2017 ([bottomB](#)). Each individual unit mass was normalised to a maximum of 1.  
952 Each period is normalised separately so the individual signal maxima on each day are  
953 visible. The graph is plotted between 200-600 mass units, with every 10 mass units  
954 averaged for simplicity. On the secondary axis is plotted PSM data, both total particle  
955 count  $>1.30$  nm (black trace) and total clusters between 1.30 and 1.84 nm (blue trace).  
956 Data is plotted at 1 hour time resolution.

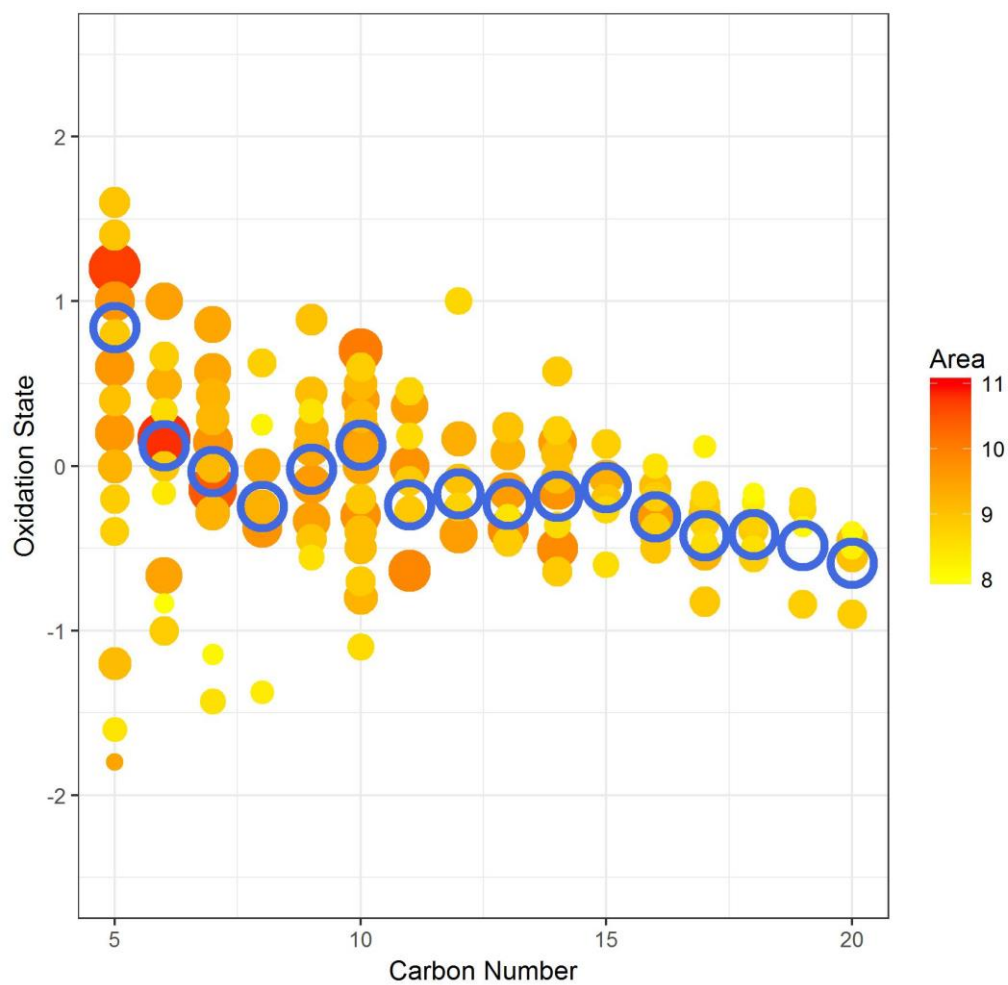
957

958 **Figure 6** SMPS + PSM contour plot for two nucleation days on 24/06/2017 and 25/06/2017. Data  
959 in bottom panel is from the PSM instrument, top panel from NanoSMPS, units in colour  
960 bar are  $\log_{10}(\text{dN}/\log D_p)$  for N in  $\text{cm}^{-3}$ . Points signify normalised sulfuric acid  
961 concentration (right axis) as measured by CI-APi-ToF.

962

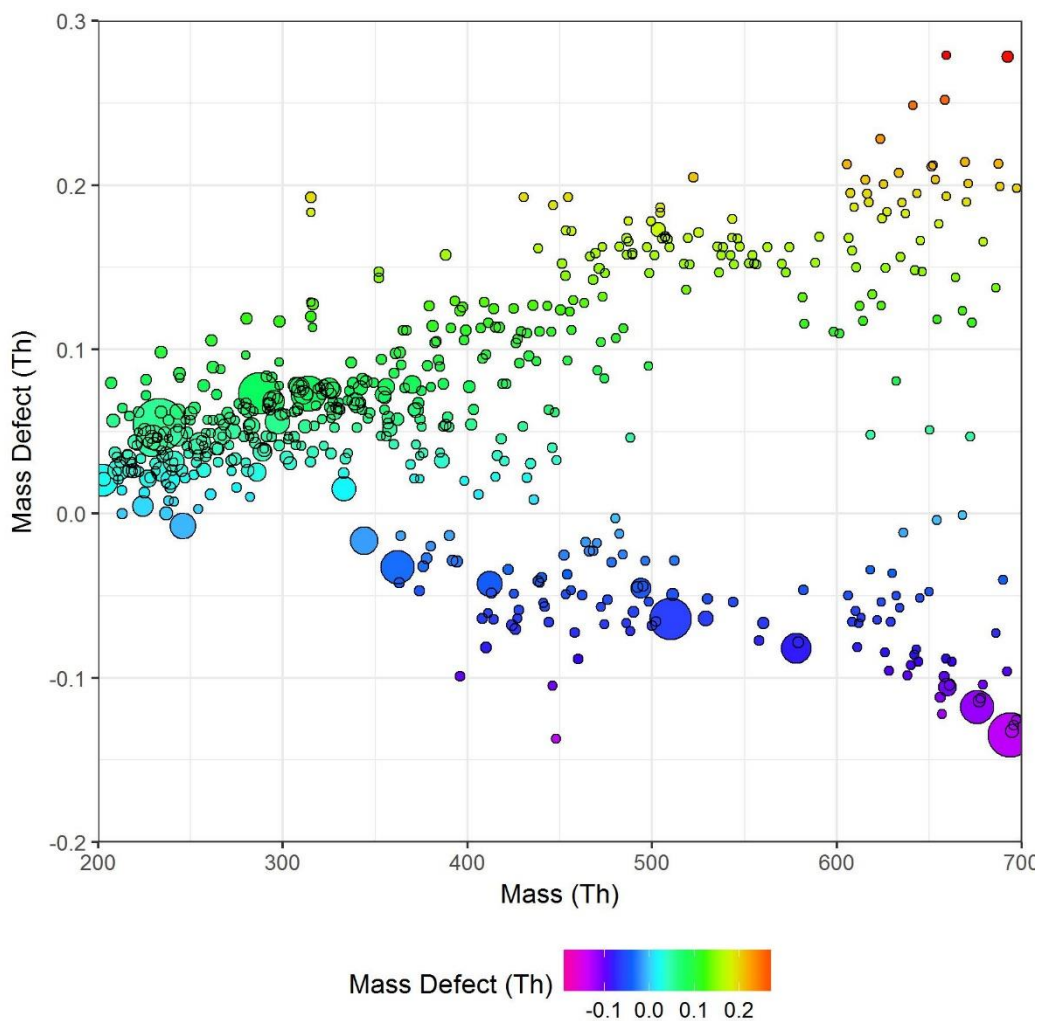
963

964

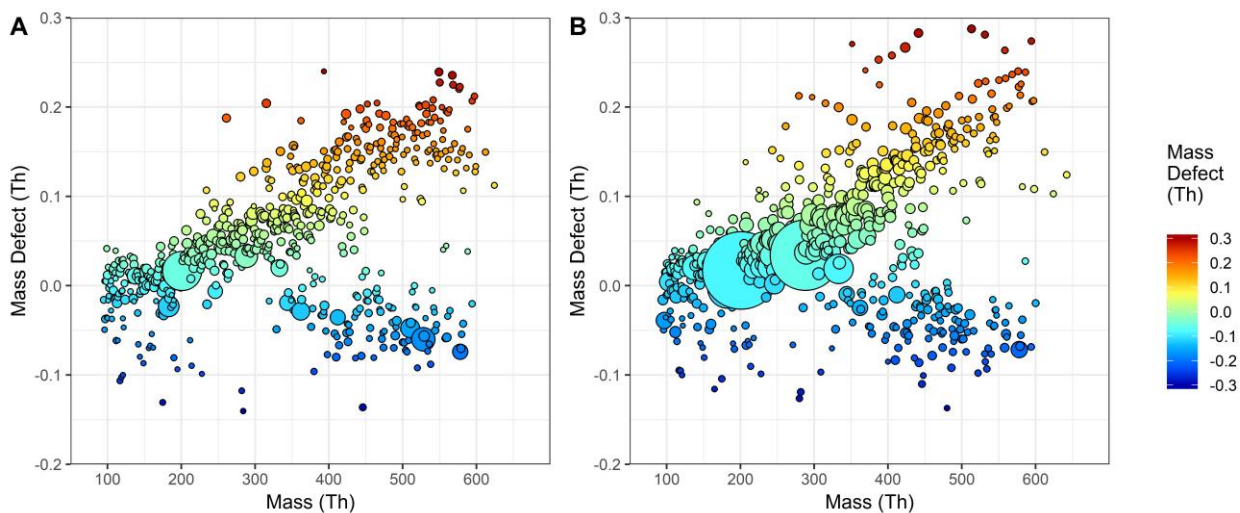


965

966 **Figure 1.** Oxidation state of carbon plotted against carbon number for (colored) individual ions and  
967 (blue circles) signal weighted average for each carbon number. Area and colour are both proportional  
968 to the peak area for each ion.



969

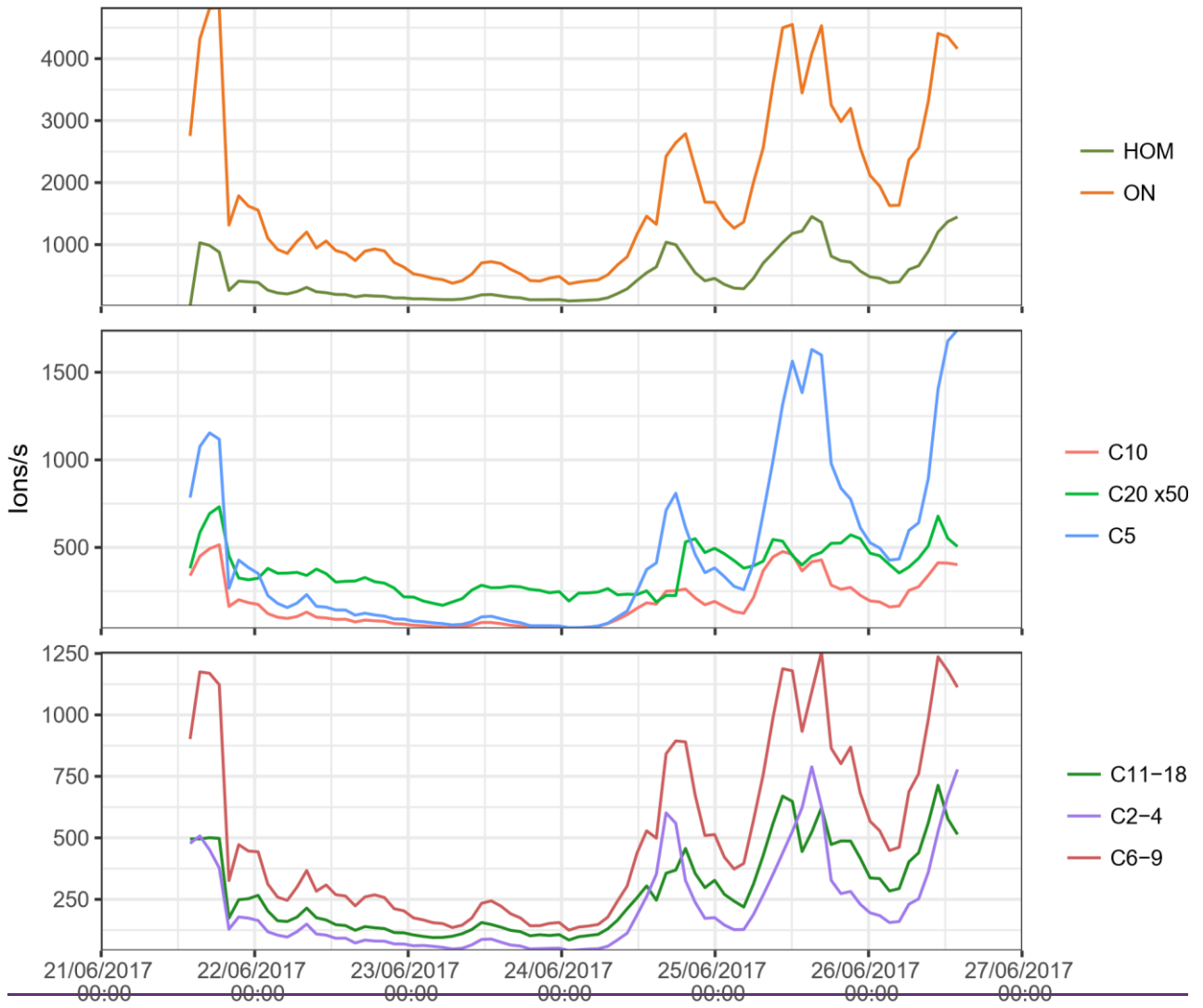


970

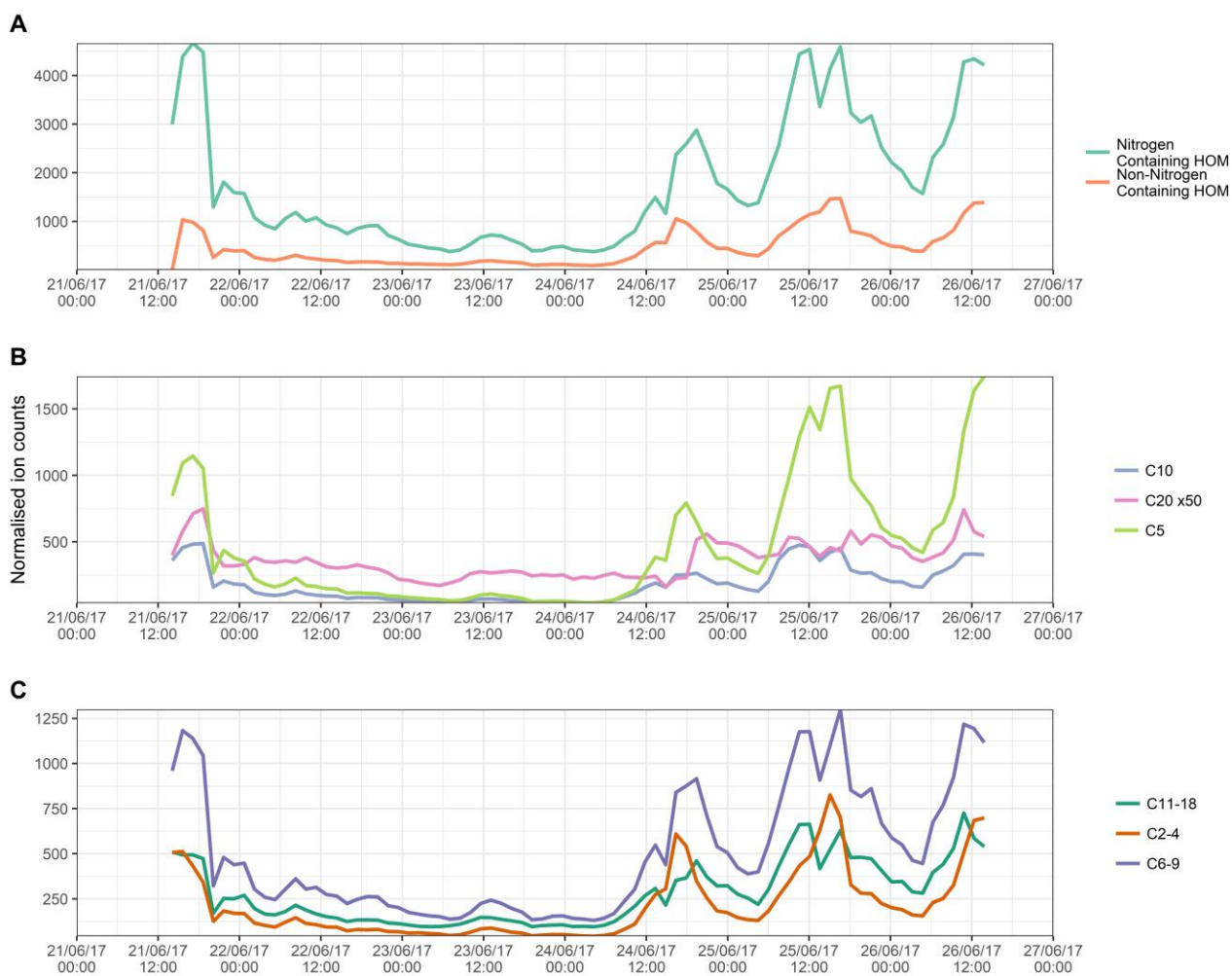
971 **Figure 2.** MKendrick mass defect plot of fitted mass spectral peaks between 100200-600700-mass  
 972 units on (a) 10:30 – 12:00 23/06/2017, a non nucleation day, and (b) 10:30 -12:00 25/06/2017, a  
 973 nucleation day, where carbon is the Kendrick base. Kendrick mass-Mass defect can be defined as the  
 974 Kendrick-mass - Kendrick-integer mass. The size of point is proportional to the signal intensity. As  
 975  $^1\text{H}$  has a positive mass defect (1.007276 Da), the upward trend along the horizontal indicates  
 976 increasing carbon chain length, and differences at similar masses are due to increasing oxygen  
 977 functionality, clustering with species such as sulfuric acid (negative mass defect) and ammonia  
 978 (positive mass defect), as  $^{16}\text{O}$  and  $^{32}\text{S}$  have negative mass defects (15.9949 and 31.9721 Da



979 respectively), while  $^{14}\text{N}$  has a positive mass defect at 14.0031 Da. Here, two ions at 201 and 288  $m/z$   
980 have been removed due to high signal.



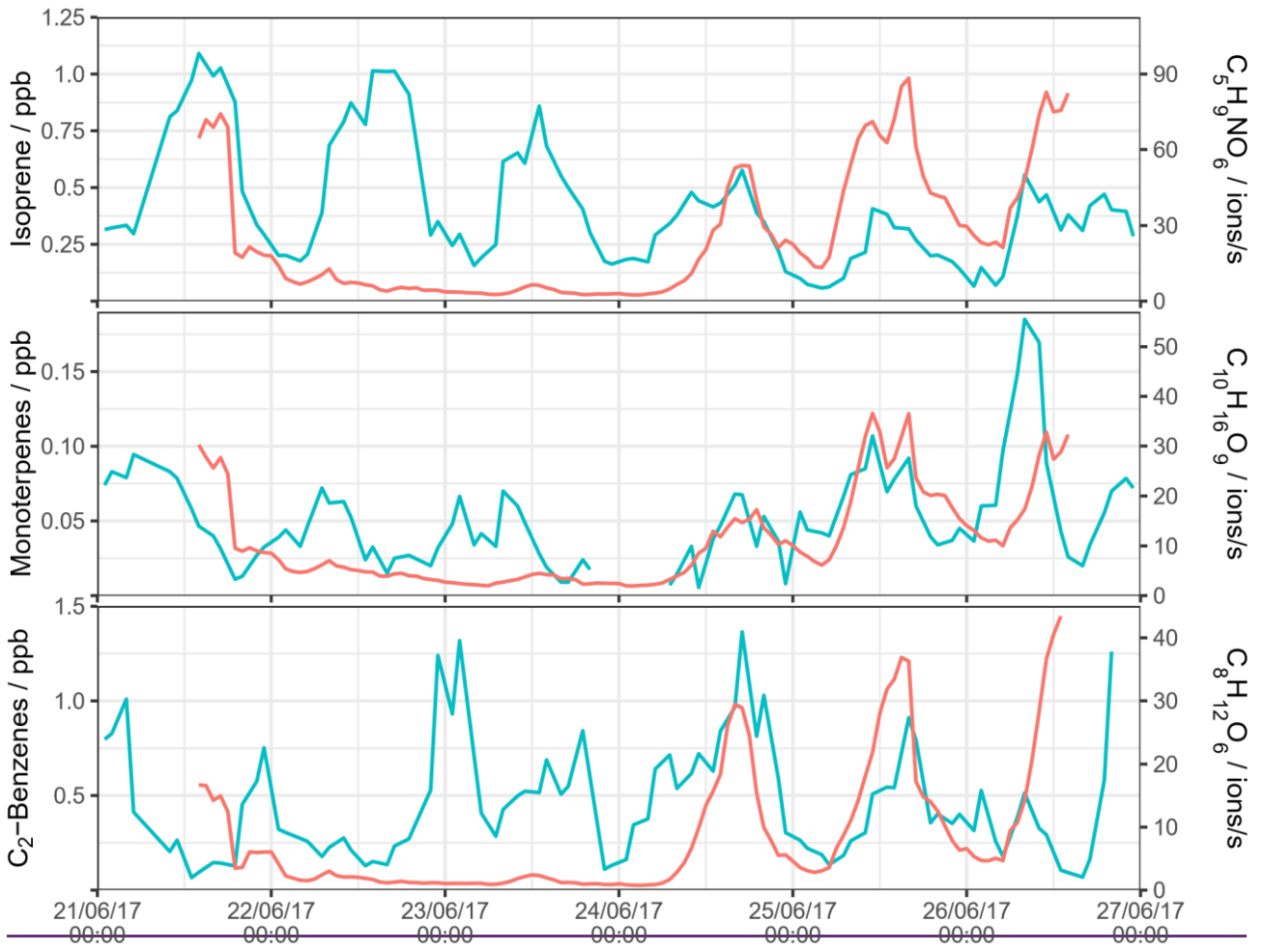
981

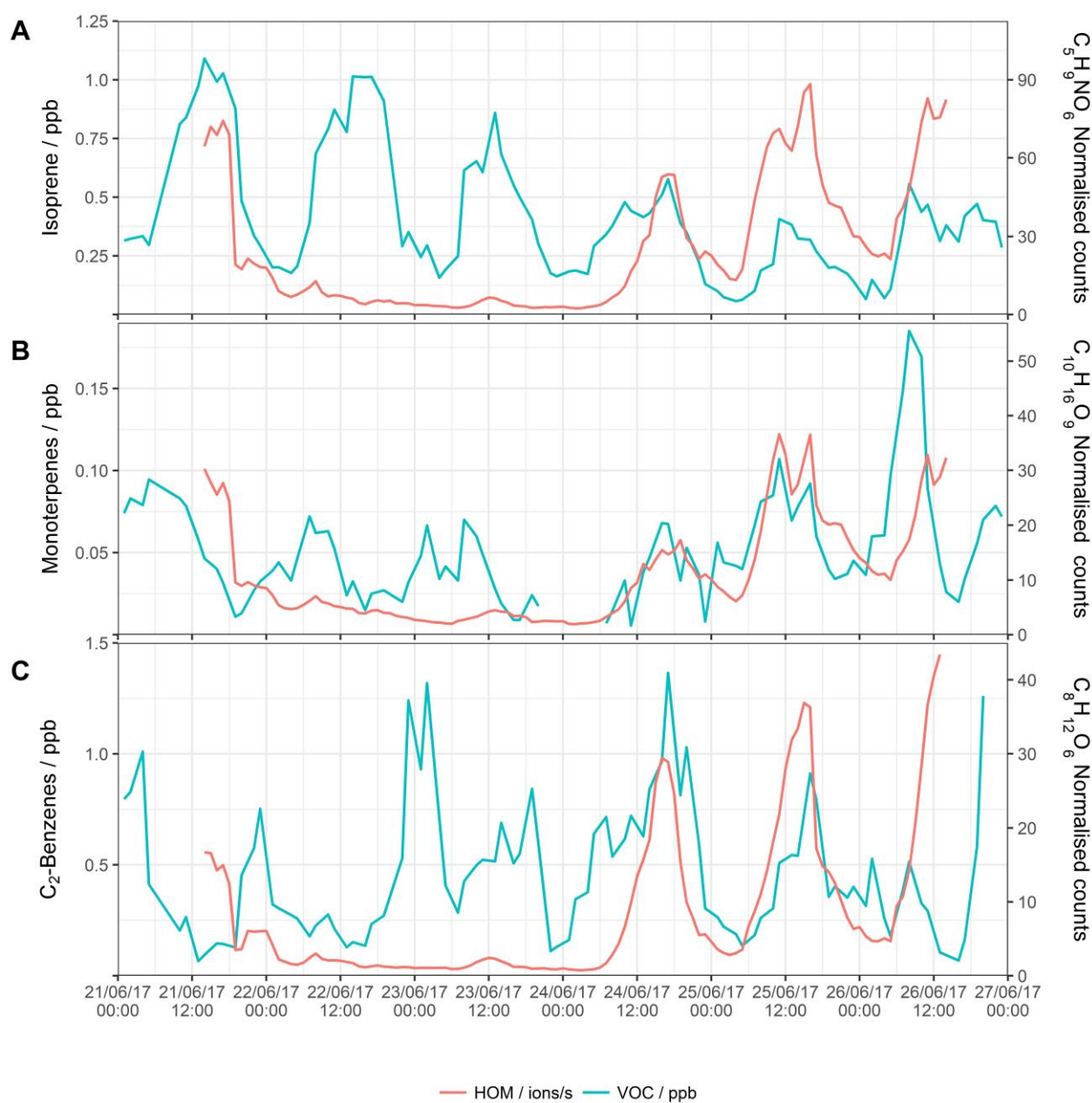


982

983 **Figure 3.** Summed time series of the concentrations of (top A) all non-nitrogen containing HOMs and  
 984 all organonitrates identified, (middle B) C5, C10 and C20 components, assumed to be dominated by  
 985 isoprene, monoterpene monomer and monoterpene dimers, signal for C20 multiplied 50 times to fit  
 986 scale, and (bottom C) summed C6 - C9 components, and summed C11 - C18 components, assumed  
 987 to be dominated by alkylbenzenes and other larger components respectively.

988





989

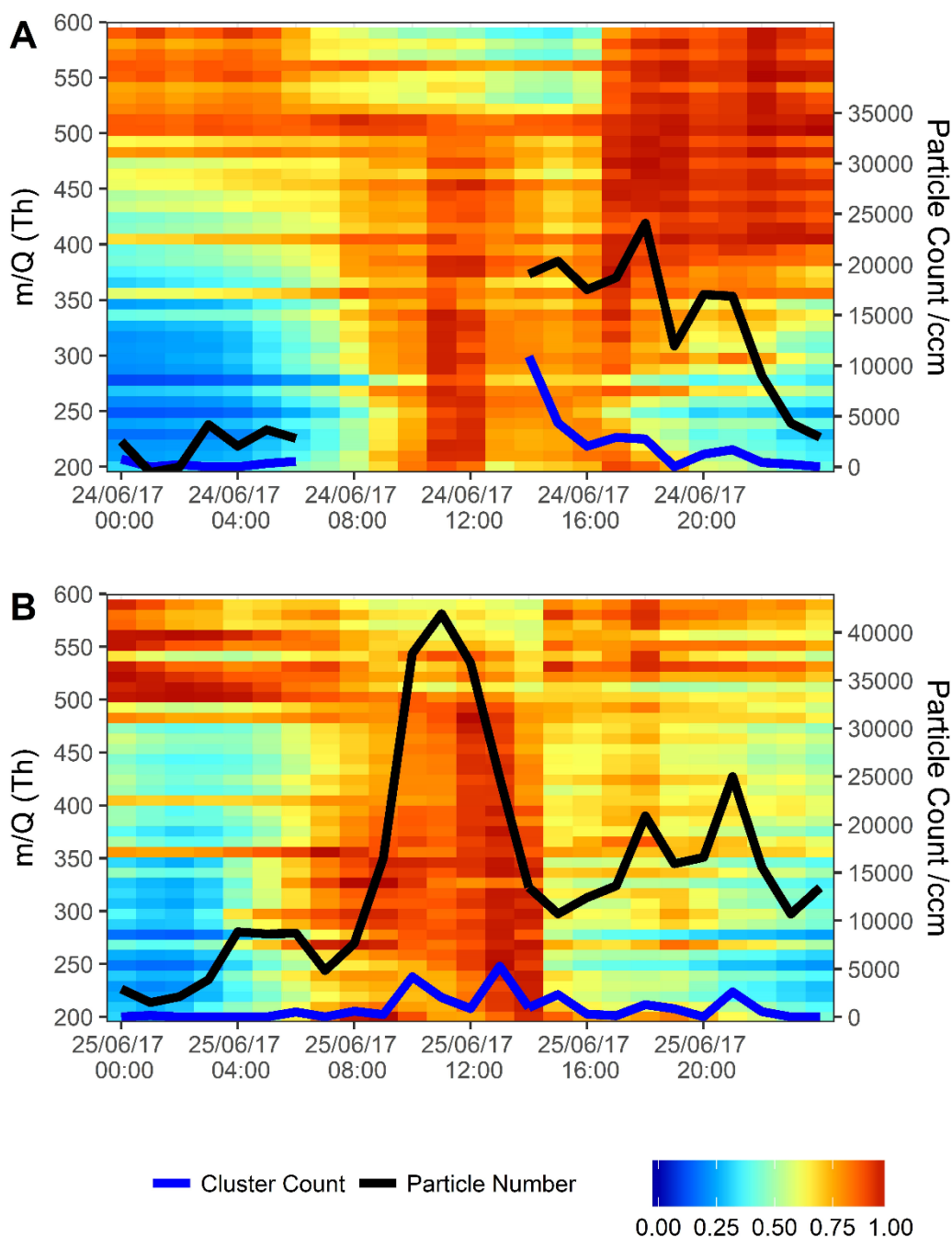
990

991 **Figure 4.** Time series for the whole sampling campaign for the concentrations of (left axis) VOCs as  
 992 measured by PTR-ToF and (right axis) a selected HOM product associated with that precursor.

993

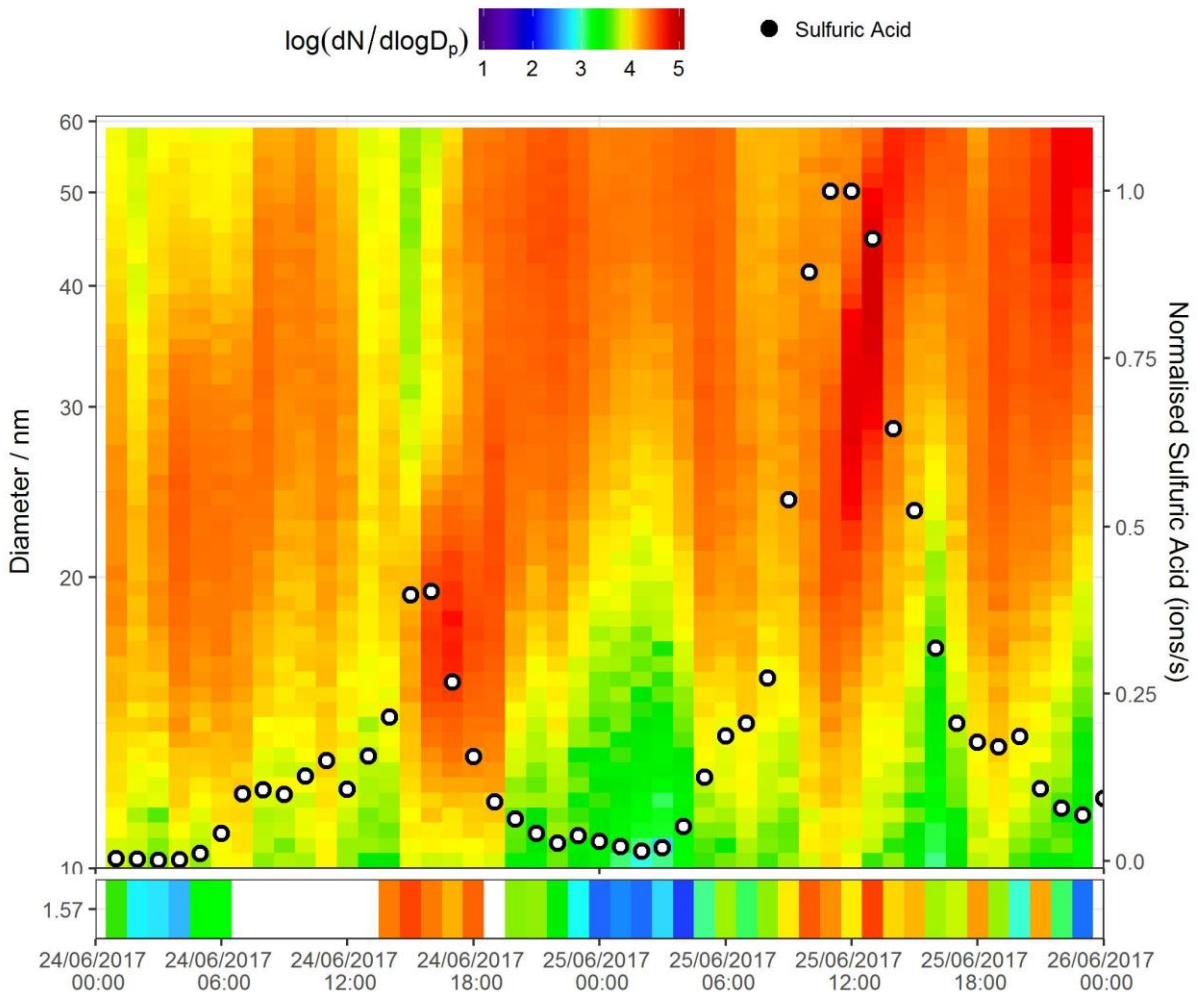
994

995

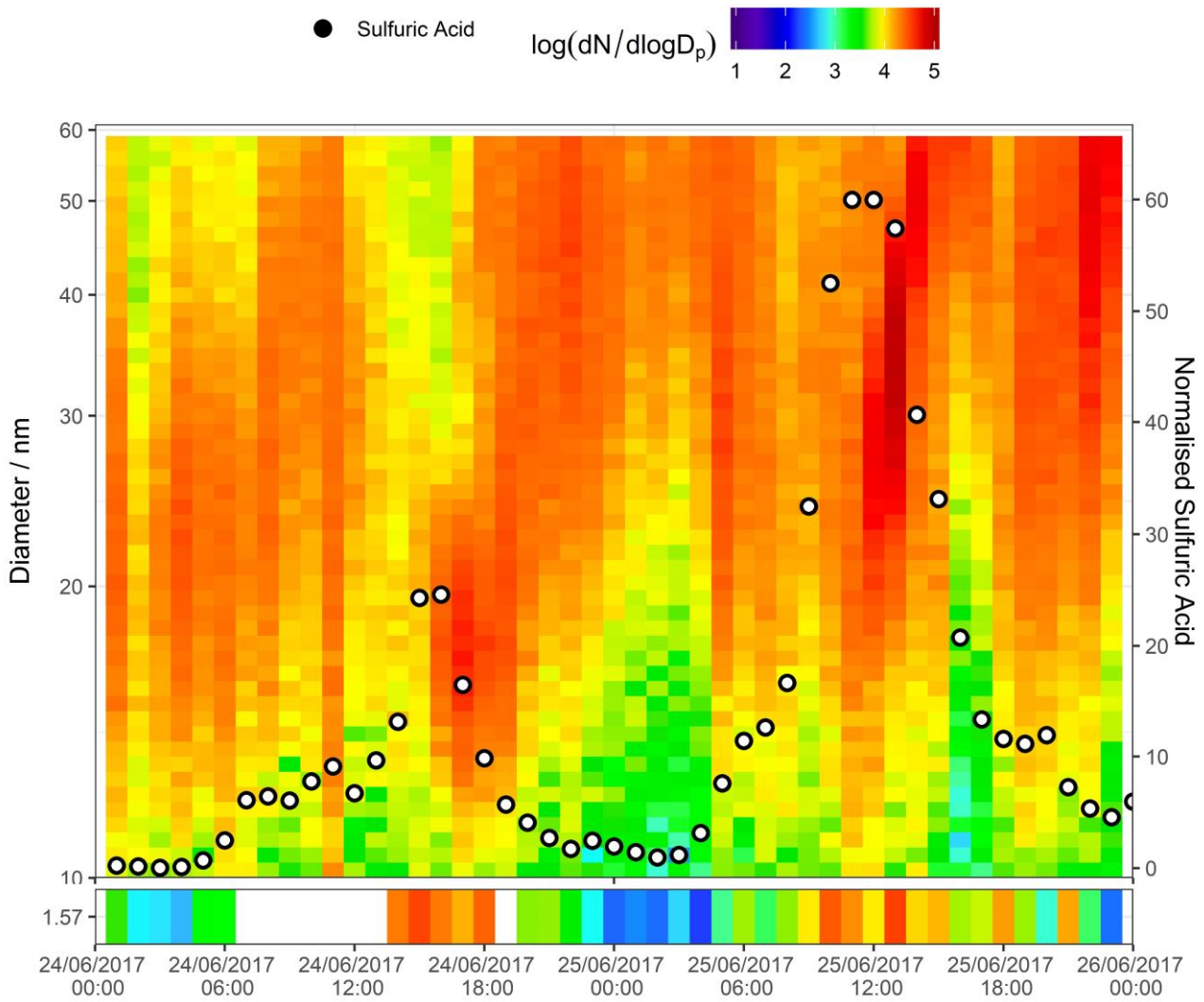


996

997 **Figure 5.** Normalised unit mass  $\text{NO}_3^-$  CI-APi-ToF signal intensity on 24/06/2017 (top A) and  
 998 25/06/2017 (bottom B). Each individual unit mass was normalised to a maximum of 1. Each period is  
 999 normalised separately so the individual signal maxima on each day are visible. The graph is plotted  
 1000 between 200-600 mass units, with every 10 mass units averaged for simplicity. On the secondary axis  
 1001 is plotted PSM data, both total particle count  $>1.30$  nm (black trace) and total clusters between 1.30  
 1002 and 1.84 nm (blue trace). Data is plotted at 1 hour time resolution.



1003



1004

1005 **Figure 6.** SMPS + PSM contour plot for two nucleation days on 24/06/2017 and 25/06/2017. Data in  
 1006 bottom panel is from the PSM instrument, top panel from NanoSMPS, units in colour bar are  $\log_{10}$   
 1007  $(dN/d\log D_p)$  for  $N$  in  $\text{cm}^{-3}$ . Points signify normalised sulfuric acid concentration (right axis) as  
 1008 measured by CI-APi-ToF.

1009

1010

1011

1012

1013

1014

1015

1 **SUPPLEMENTARY MATERIAL**

2

3 **OBSERVATIONS OF HIGHLY OXIDISED**  
4 **MOLECULES AND PARTICLE NUCLEATION**  
5 **IN THE ATMOSPHERE OF BEIJING**

6

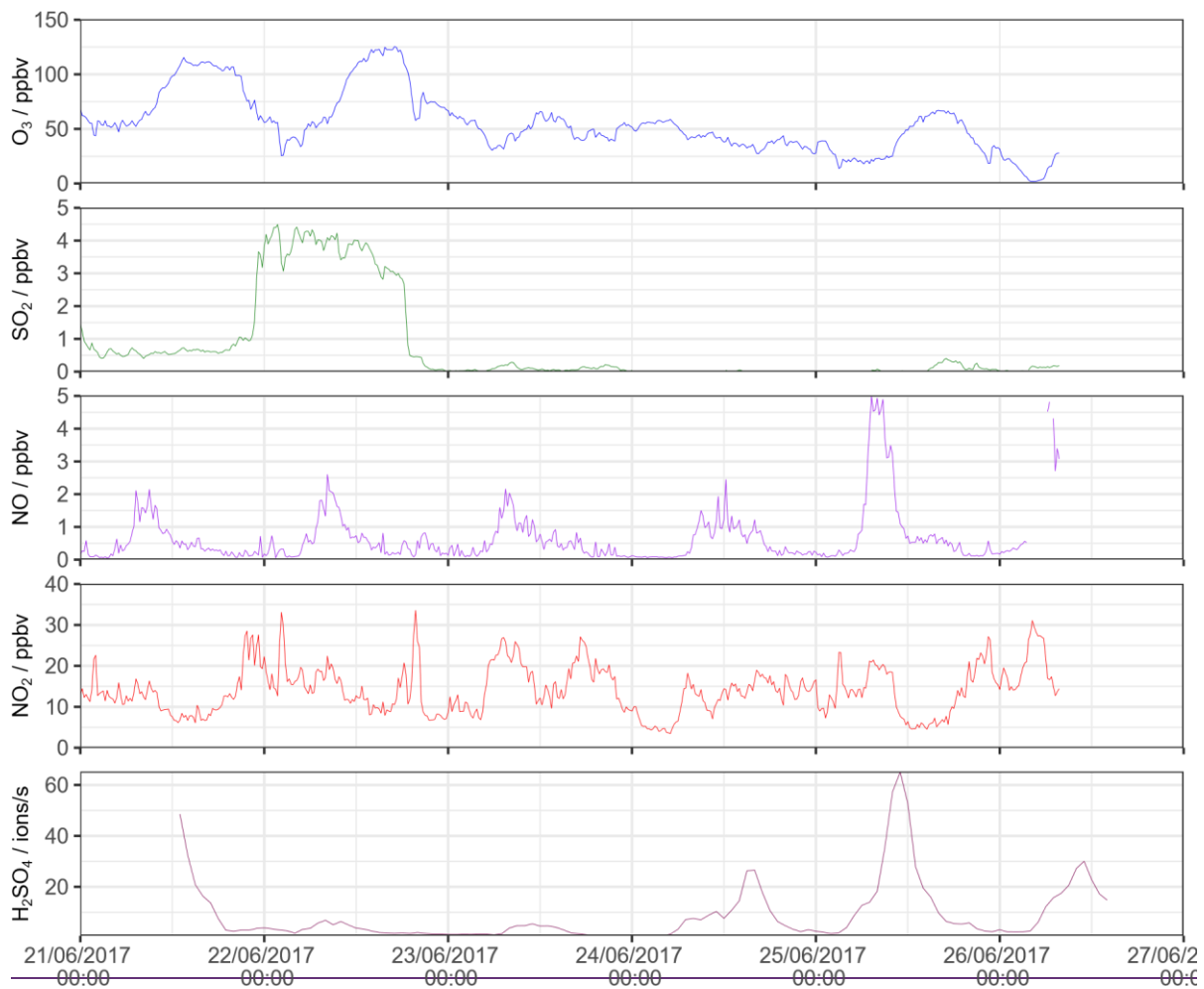
7 **James Brean, Roy M. Harrison, Zongbo Shi**

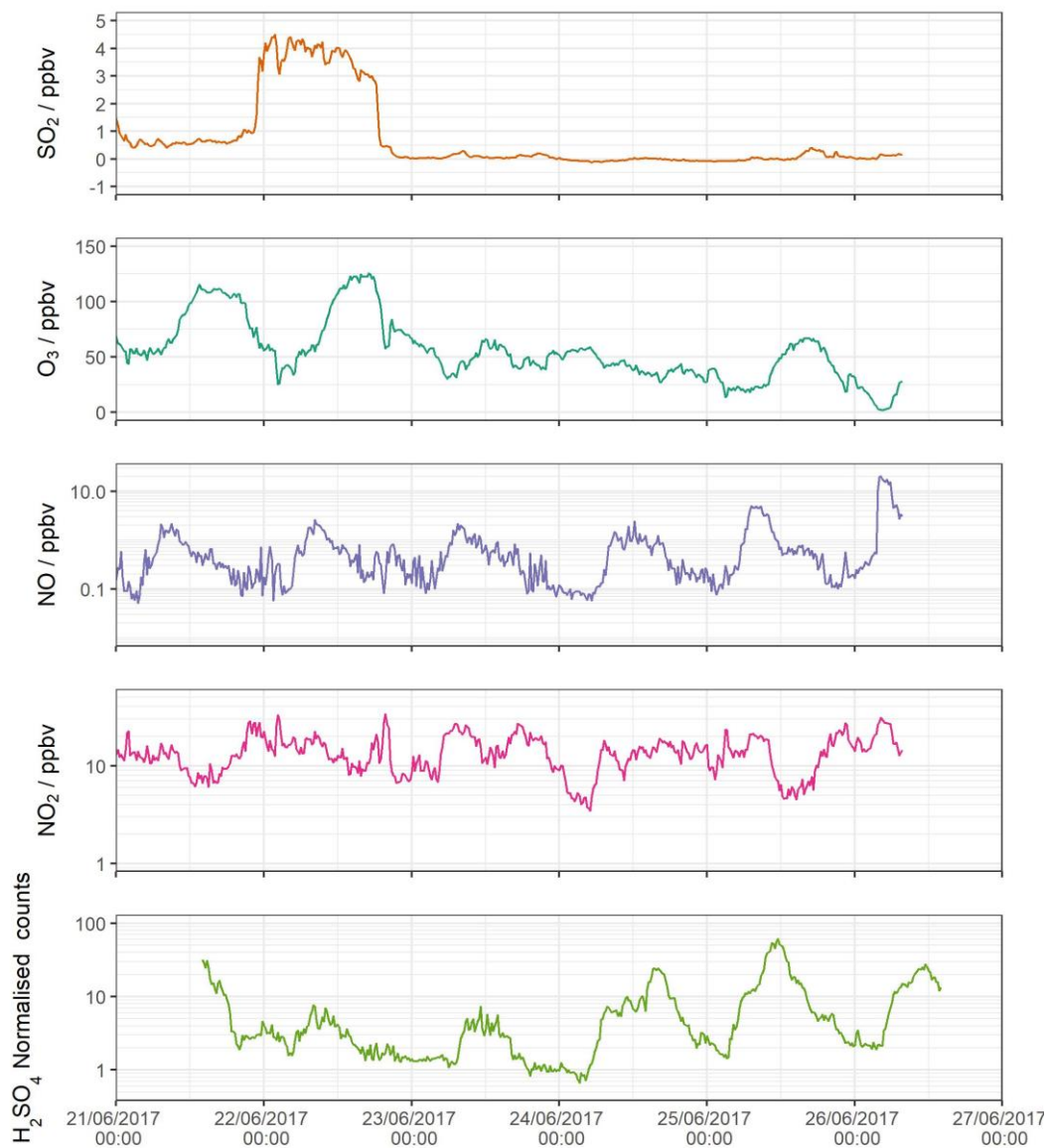
8 **David C.S. Beddows, W. Joe F. Acton~~and~~**

9 **C. Nicholas Hewitt, Freya A. Squires and James Lee**

10

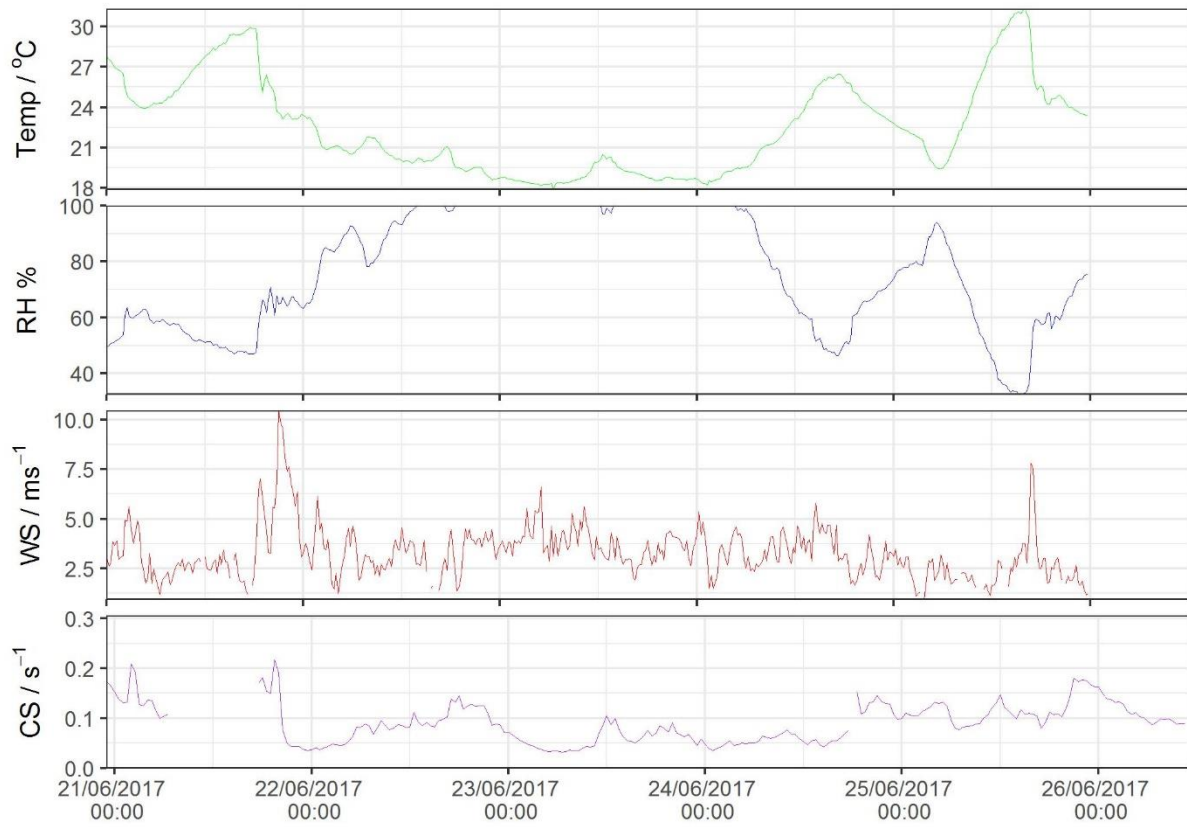


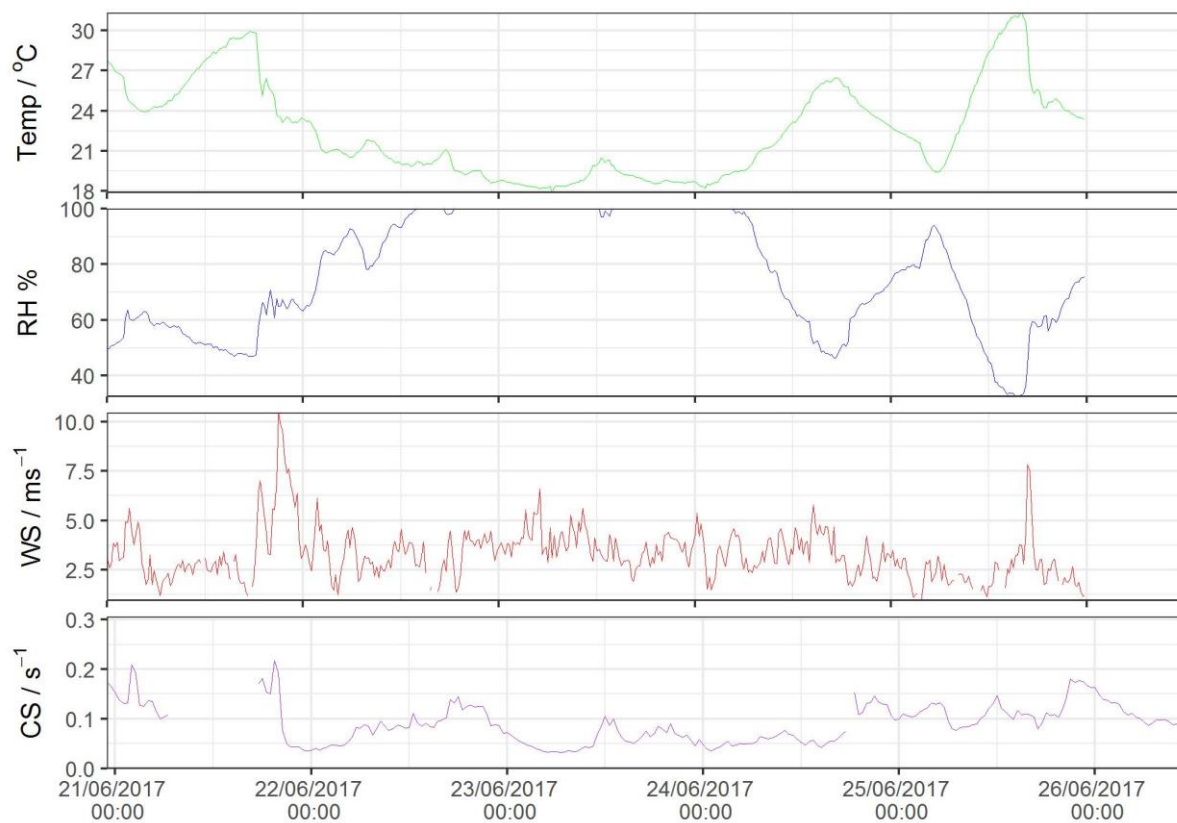




12

13 **Figure S1.** Time series for (from top downwards), SO<sub>2</sub>, O<sub>3</sub>, NO, NO<sub>2</sub> and H<sub>2</sub>SO<sub>4</sub>. Time series for  
 14 (from top downwards), O<sub>3</sub>, SO<sub>2</sub>, NO, NO<sub>2</sub> and H<sub>2</sub>SO<sub>4</sub>. Data for O<sub>3</sub>, SO<sub>2</sub>, NO and NO<sub>2</sub> are taken  
 15 from Shi et al. (2019), and for H<sub>2</sub>SO<sub>4</sub> are from this study.  
 16





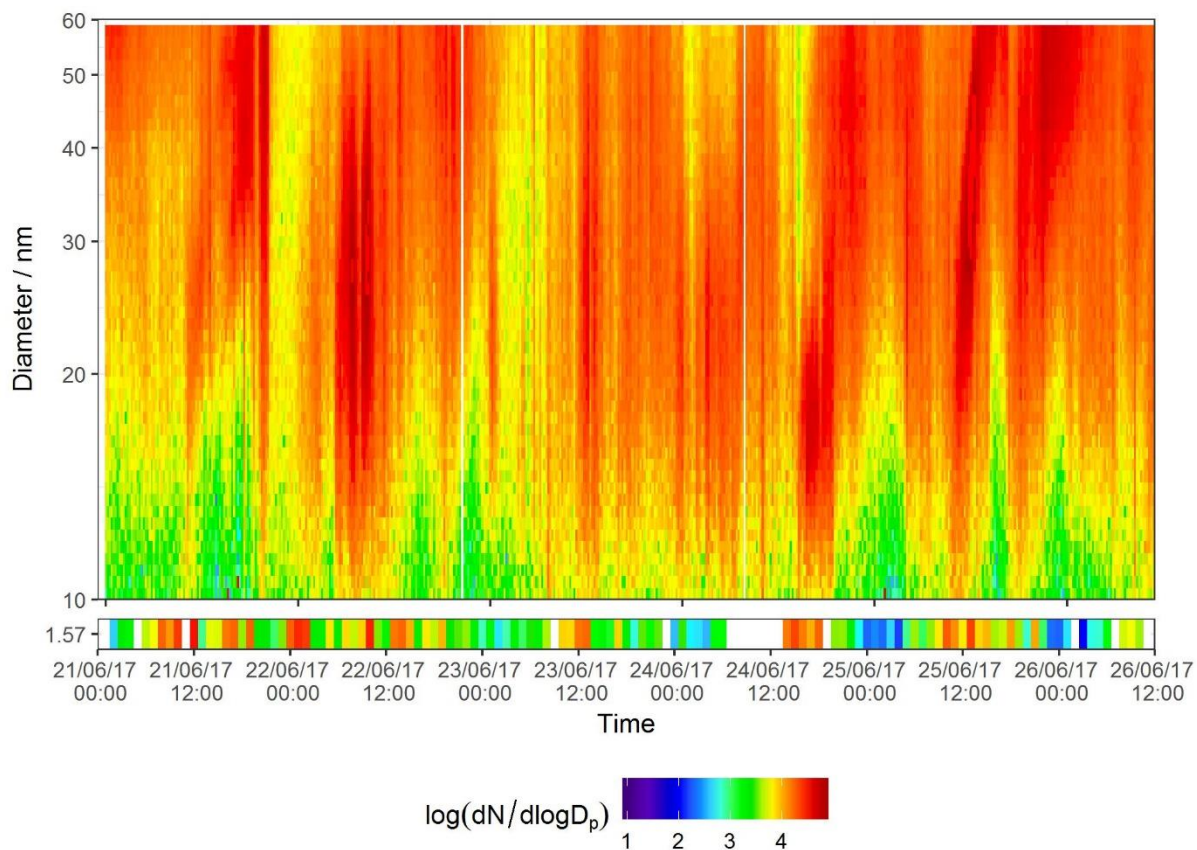
18  
19  
20  
21  
22  
23

---

**Figure S2.** MET data for the sampling period. Temperature, relative humidity and wind speed were collected at 120 m on the meteorological tower at the sampling site. The particle size distribution from which condensation sink was calculated was measured at 2 metres.

24

25



26

27 **Figure S3.** SMPS + PSM contour plot for all days of sampling period. Data, from top panel to  
28 bottom, from long column SMPS, nano column SMPS and PSM instruments, units in colour bar  
29 are  $\log_{10}(dN/d\log D_p)$  for N in  $\text{cm}^{-3}$ .

30

31

32 **Table S1.** Relationship between molecular mass and calculated electrical mobility diameter (nm)  
 33 for multiple masses up to 800 Da and densities , as calculated according to Tammet (1995), and  
 34 corrected according to Larriba et al. (2011).

Mass / Da	$\rho$ g/cm <sup>3</sup>					
	1.0	1.2	1.4	1.6	1.8	2.0
200	1.159	1.109	1.068	1.035	1.006	0.982
300	1.284	1.226	1.179	1.141	1.109	1.081
400	1.383	1.319	1.268	1.226	1.19	1.159
500	1.466	1.397	1.342	1.297	1.259	1.226
600	1.539	1.466	1.408	1.359	1.319	1.284
700	1.605	1.528	1.466	1.415	1.372	1.335
800	1.664	1.583	1.519	1.466	1.421	1.383

35

36 **Table S2.** All peaks identified by NO<sub>3</sub>- CIMS

37

Ion	Mass
C <sub>2</sub> HO <sub>3</sub> O <sup>-</sup>	88.988
C <sub>3</sub> H <sub>5</sub> O <sub>2</sub> O <sup>-</sup>	89.025
<u>CH<sub>3</sub>SO<sub>3</sub><sup>-</sup></u>	<u>94.98</u>
HSO <sub>4</sub> <sup>-</sup>	96.96
C <sub>4</sub> H <sub>3</sub> O <sub>2</sub> O <sup>-</sup>	99.009
C <sub>4</sub> H <sub>5</sub> O <sub>2</sub> O <sup>-</sup>	101.024
C <sub>3</sub> H <sub>3</sub> O <sub>3</sub> O <sup>-</sup>	103.004
SO <sub>4</sub> O <sup>-</sup>	111.947
C <sub>6</sub> H <sub>4</sub> NO <sub>3</sub> <sup>-</sup>	138.019
SO <sub>3</sub> NO <sub>3</sub> <sup>-</sup>	141.945
<del>C<sub>2</sub>H<sub>7</sub>N HSO<sub>4</sub><sup>-</sup></del>	<del>142.018</del>
C <sub>5</sub> H <sub>9</sub> O <sub>4</sub> O <sup>-</sup>	149.046
H <sub>2</sub> SO <sub>4</sub> NO <sub>3</sub> <sup>-</sup>	159.956
C <sub>3</sub> H <sub>5</sub> NO <sub>3</sub> NO <sub>3</sub> <sup>-</sup>	165.015
C <sub>3</sub> H <sub>4</sub> O <sub>4</sub> NO <sub>3</sub> <sup>-</sup>	165.999
C <sub>8</sub> H <sub>11</sub> O <sub>3</sub> O <sup>-</sup>	171.066
C <sub>7</sub> H <sub>10</sub> NO <sub>3</sub> O <sup>-</sup>	172.062
IO <sub>3</sub> <sup>-</sup>	174.89
C <sub>4</sub> H <sub>6</sub> O <sub>4</sub> NO <sub>3</sub> <sup>-</sup>	180.015
C <sub>3</sub> H <sub>6</sub> NO <sub>4</sub> NO <sub>3</sub> <sup>-</sup>	182.018
C <sub>4</sub> H <sub>6</sub> O <sub>2</sub> HSO <sub>4</sub> <sup>-</sup>	182.997
C <sub>3</sub> H <sub>6</sub> O <sub>5</sub> NO <sub>3</sub> <sup>-</sup>	184.01
C <sub>3</sub> H <sub>5</sub> O <sub>3</sub> HSO <sub>4</sub> <sup>-</sup>	185.984
C <sub>5</sub> H <sub>6</sub> NO <sub>3</sub> NO <sub>3</sub> <sup>-</sup>	191.031
C <sub>5</sub> H <sub>8</sub> O <sub>4</sub> NO <sub>3</sub> <sup>-</sup>	194.031
H <sub>2</sub> SO <sub>4</sub> HSO <sub>4</sub> <sup>-</sup>	194.926

38 **Table S2** continued

Ion	Mass
$C_4H_8O_5NO_3^-$	198.026
$C_5H_{10}O_2HSO_4^-$	199.028
$C_6H_5NO_3NO_3^-$	201.015
$HNO_3 SO_3 NO_3^-$	204.941
$C_6H_{12}NO_3NO_3^-$	208.07
$C_5H_9NO_4NO_3^-$	209.042
$C_5H_8O_5NO_3^-$	210.026
$C_4H_7NO_5NO_3^-$	211.021
$C_5H_{10}O_5NO_3^-$	212.041
$C_4H_8O_6NO_3^-$	214.02
$C_7H_7NO_3NO_3^-$	215.031
$C_4H_{10}O_6NO_3^-$	216.036
$C_7H_8O_4NO_3^-$	218.031
$C_6H_7NO_4NO_3^-$	219.026
$C_7H_{10}O_4NO_3^-$	220.046
$C_6H_9NO_4NO_3^-$	221.042
$C_5H_7NO_5NO_3^-$	223.021
$C_9H_9NO_2NO_3^-$	225.052
$C_{10}H_{13}NONO_3^-$	225.088
$C_4H_7NO_6NO_3^-$	227.016
$C_8H_9NO_3NO_3^-$	229.047
$C_5H_{12}O_6NO_3^-$	230.052
$C_7H_7NO_4NO_3^-$	231.026



40 **Table S2** continued

Ion	Mass
$C_8H_{10}O_4NO_3^-$	232.046
$C_7H_9NO_4NO_3^-$	233.042
$C_7H_8O_5NO_3^-$	234.026
$C_7H_{10}O_5NO_3^-$	236.041
$C_5H_5NO_6NO_3^-$	237.000
$C_6H_9NO_5NO_3^-$	237.036
$C_6H_8O_6NO_3^-$	238.020
$C_7H_{12}O_5NO_3^-$	238.057
$C_5H_7NO_6NO_3^-$	239.016
$C_{10}H_{11}NO_2NO_3^-$	239.067
$C_6H_{10}O_6NO_3^-$	240.036
$C_5H_9NO_6NO_3^-$	241.031
$C_5H_{11}NO_6NO_3^-$	243.047
$C_5H_{10}O_7NO_3^-$	244.031
$C_{10}H_{14}O_3NO_3^-$	244.083
<del><math>(H_2SO_4)_3NH_3HS</math></del>	<del>246.007</del>
$\ominus_4^-$	
$C_3H_7NO_8NO_3^-$	247.006
$C_8H_{10}O_5NO_3^-$	248.041
$C_7H_9NO_5NO_3^-$	249.036
$C_8H_{12}O_5NO_3^-$	250.057
$C_6H_9NO_6NO_3^-$	253.031
$C_5H_8N_2O_6NO_3^-$	254.027

Ion	Mass
$\text{C}_{10}\text{H}_{11}\text{NO}_2\text{NO}_3^-$	239.067
$\text{C}_6\text{H}_{10}\text{O}_6\text{NO}_3^-$	240.036
$\text{C}_5\text{H}_9\text{NO}_6\text{NO}_3^-$	241.031
$\text{C}_5\text{H}_{11}\text{NO}_6\text{NO}_3^-$	243.047
$\text{C}_5\text{H}_{10}\text{O}_7\text{NO}_3^-$	244.031
$\text{C}_{10}\text{H}_{14}\text{O}_3\text{NO}_3^-$	244.083
<del><math>(\text{H}_2\text{SO}_4)_3\text{NH}_3\text{HSO}_4^-</math></del>	<del>246.007</del>
$\text{C}_3\text{H}_7\text{NO}_8\text{NO}_3^-$	247.006
$\text{C}_8\text{H}_{10}\text{O}_5\text{NO}_3^-$	248.041
$\text{C}_7\text{H}_9\text{NO}_5\text{NO}_3^-$	249.036
$\text{C}_8\text{H}_{12}\text{O}_5\text{NO}_3^-$	250.057
$\text{C}_6\text{H}_9\text{NO}_6\text{NO}_3^-$	253.031
$\text{C}_8\text{H}_{12}\text{O}_6\text{NO}_3^-$	266.052
$\text{C}_5\text{H}_{10}\text{O}_9\text{NO}_3^-$	276.021
$\text{C}_{10}\text{H}_{14}\text{O}_5\text{NO}_3^-$	276.072
$\text{C}_7\text{H}_7\text{NO}_3\text{HNO}_3\text{NO}_3^-$	278.027
$\text{C}_8\text{H}_{12}\text{O}_7\text{NO}_3^-$	282.047
$\text{C}_6\text{H}_{10}\text{N}_2\text{O}_7\text{NO}_3^-$	284.037
$\text{C}_{10}\text{H}_9\text{NO}_5\text{NO}_3^-$	285.036
$\text{C}_{10}\text{H}_8\text{O}_6\text{NO}_3^-$	286.02
$\text{C}_5\text{H}_{10}\text{N}_2\text{O}_8\text{NO}_3^-$	288.032
$\text{C}_{10}\text{H}_{15}\text{NO}_5\text{NO}_3^-$	291.083
$\text{C}_{10}\text{H}_{14}\text{O}_6\text{NO}_3^-$	292.067
$\text{C}_9\text{H}_{13}\text{NO}_6\text{NO}_3^-$	293.063
$\text{C}_{10}\text{H}_{16}\text{O}_6\text{NO}_3^-$	294.083
$\text{C}_9\text{H}_{15}\text{NO}_6\text{NO}_3^-$	295.078
$\text{C}_2\text{H}_7\text{NHNO}_3\text{NO}_3^-$	296.033
$\text{C}_{12}\text{H}_{13}\text{NO}_4\text{NO}_3^-$	297.073
$\text{C}_6\text{H}_{10}\text{N}_2\text{O}_8\text{NO}_3^-$	300.032



44 **Table S2** continued

Ion	Mass
$C_7H_{12}O_9NO_3^-$	302.036
$C_5H_{10}N_2O_9NO_3^-$	304.027
$C_{11}H_{17}NO_5NO_3^-$	305.099
$C_{10}H_{15}NO_6NO_3^-$	307.078
$HSO_5H_2SO_4HSO_4^-$	307.882
$C_{10}H_{14}O_7NO_3^-$	308.062
$C_{13}H_{13}NO_4NO_3^-$	309.073
$C_{13}H_{14}NO_4NO_3^-$	310.081
$C_9H_{15}NO_7NO_3^-$	311.073
$C_9H_{14}O_8NO_3^-$	312.057
$C_7H_{12}N_2O_8NO_3^-$	314.048
$C_{10}H_9NO_7NO_3^-$	317.026
$C_{11}H_{12}O_7NO_3^-$	318.047
$C_{10}H_{15}N_2O_6NO_3^-$	321.081
<del><math>HNO_3 \cdot HSO_5 \cdot (NH_3)_3</math></del>	<del>323.99</del>
<del><math>HSO_4^-</math></del>	
$C_{10}H_{14}O_8NO_3^-$	324.057
$C_{10}H_{17}NO_7NO_3^-$	325.089
$C_{10}H_{16}O_8NO_3^-$	326.073
$C_9H_{15}NO_8NO_3^-$	327.068
$C_{13}H_{14}O_6NO_3^-$	328.067
$C_{12}H_{13}NO_6NO_3^-$	329.063
$C_{11}H_{12}N_2O_6NO_3^-$	330.058
$(C_2H_7N)_3H_2SO_4HSO_4^-$	330.101
$C_{10}H_9NO_8NO_3^-$	333.021

45

46

47 **Table S2** continued

Ion	Mass
$C_9H_8N_2O_8NO_3^-$	334.016
$C_{10}H_{11}NO_8NO_3^-$	335.037
$H_2OHSO_5NH_3(HNO_3)_2NO_3^-$	<del>335.971</del>
$C_{11}H_{17}NO_7NO_3^-$	337.089
$C_{11}H_{16}O_8NO_3^-$	338.073
$C_{10}H_{15}NO_8NO_3^-$	339.068
$C_{14}H_{14}O_6NO_3^-$	340.067
$C_{10}H_{16}O_9NO_3^-$	342.068
$(H_2SO_4)_2(NH_3)_3HSO_4^-$	<del>343.975</del>
$C_{13}H_{17}NO_6NO_3^-$	345.094
$C_2H_7NHNO_3_2HSO_5NO_3^-$	345.992
$C_{11}H_{11}NO_8NO_3^-$	347.037
$C_{10}H_{14}N_2O_8NO_3^-$	352.063
$C_{11}H_{17}NO_8NO_3^-$	353.084
$C_{14}H_{14}NO_6NO_3^-$	354.07
$C_{10}H_{15}NO_9NO_3^-$	355.063
$C_{11}H_{18}O_9NO_3^-$	356.083
$C_{12}H_{12}N_2O_7NO_3^-$	358.053
$C_{14}H_{19}NO_6NO_3^-$	359.11
$H_2O(NH_3)_2HSO_5H_2SO_4HSO_4^-$	<del>359.946</del>
$H_2O(NH_3)_3(H_2SO_4)_2HSO_4^-$	<del>361.985</del>
$(H_2O)_2(NH_3)_2(H_2SO_4)_2HSO_4^-$	<del>362.969</del>
$C_{13}H_{19}NO_7NO_3^-$	363.105
$C_{13}H_{18}O_8NO_3^-$	364.089
$C_{13}H_{20}O_8NO_3^-$	366.104
$C_{12}H_{19}NO_8NO_3^-$	367.099

48

49 **Table S2** continued

Ion	Mass
$C_{11}H_{16}O_{10}NO_3^-$	370.063
$C_{14}H_{15}NO_7NO_3^-$	371.073
$C_{14}H_{14}O_8NO_3^-$	372.057
$C_{13}H_{13}NO_8NO_3^-$	373.052
$(H_2O)_2NH_3(H_2SO_4)_2$	373.966
$HNO_3NO_3^-$	
$C_{10}H_{16}O_{11}NO_3^-$	374.058
$(C_2H_7N)_2(H_2SO_4)_2HSO_4^-$	383.011
$C_{13}H_{15}NO_8NO_3^-$	375.068
$H_2O(NH_3)_3HSO_5$	376.972
$H_2SO_4HSO_4^-$	
$(H_2O)_2(NH_3)_2HSO_5$	377.956
$H_2SO_4HSO_4^-$	
$C_{14}H_{23}NO_7NO_3^-$	379.136
$C_{13}H_{21}NO_8NO_3^-$	381.115
$C_{16}H_{18}NO_6NO_3^-$	382.102
$C_{16}H_{19}NO_6NO_3^-$	383.11
$C_{14}H_{15}NO_8NO_3^-$	387.068
$C_{10}H_{17}NO_{11}NO_3^-$	389.069
$C_{15}H_{23}NO_7NO_3^-$	391.136
$C_{14}H_{21}NO_8NO_3^-$	393.115
$C_{17}H_{21}NO_6NO_3^-$	397.125

50

51

52 **Table S2** continued

Ion	Mass
$C_{16}H_{20}N_2O_6NO_3^-$	398.121
$C_{16}H_{19}NO_7NO_3^-$	399.105
$C_{16}H_{18}O_8NO_3^-$	400.089
$C_{15}H_{17}NO_8NO_3^-$	401.084
$C_{15}H_{16}O_9NO_3^-$	402.068
$C_{14}H_{15}NO_9NO_3^-$	403.063
$C_{17}H_{28}O_7NO_3^-$	406.172
$C_{17}H_{18}N_2O_6NO_3^-$	408.105
$C_{18}H_{21}NO_6NO_3^-$	409.125
$C_{17}H_{19}NO_7NO_3^-$	411.105
$C_{17}H_{20}O_8NO_3^-$	414.104
$C_{16}H_{19}NO_8NO_3^-$	415.099
$C_{16}H_{21}NO_8NO_3^-$	417.115
$C_{14}H_{14}O_{11}NO_3^-$	420.042
<del><math>(NH_3)_2(H_2SO_4)_3HSO_4^-</math></del>	<del>424.915</del>
$C_{18}H_{21}NO_7NO_3^-$	425.12
$C_{15}H_{24}O_{10}NO_3^-$	426.125
<del><math>(C_2H_7N)_2(H_2SO_4)_2HSO_4^-</math></del>	<del>428.068</del>
$C_{18}H_{22}O_8NO_3^-$	428.12
$C_{17}H_{21}NO_8NO_3^-$	429.115
$C_{16}H_{23}NO_9NO_3^-$	435.126
<del><math>C_2H_7N(H_2SO_4)_3HSO_4^-</math></del>	<del>435.919</del>

53

Ion	Mass
$C_{15}H_{23}NO_{10}NO_3^-$	439.121
<del><math>(H_2SO_4)_3(NH_3)_3HSO_4^-</math></del>	<del>441.942</del>
$C_{18}H_{23}NO_8NO_3^-$	443.131
$C_{12}H_{16}O_{14}NO_3^-$	446.042
$C_{17}H_{27}NO_9NO_3^-$	451.157
$C_{16}H_{25}NO_{10}NO_3^-$	453.136
$C_{17}H_{28}O_{10}NO_3^-$	454.157
$C_{16}H_{27}NO_{10}NO_3^-$	455.152
$C_{19}H_{22}O_9NO_3^-$	456.115
<del><math>(NH_3)_2HSO_5(H_2SO_4)_2HSO_4^-</math></del>	<del>456.929</del>
$C_{15}H_{25}NO_{11}NO_3^-$	457.131
<del><math>H_2O(NH_3)_2HSO_5(H_2SO_4)_2HSO_4^-</math></del>	<del>457.913</del>
$C_{20}H_{32}NO_7NO_3^-$	460.206
$C_{17}H_{25}NO_{10}NO_3^-$	465.136
$C_{17}H_{29}NO_{10}NO_3^-$	469.168
$C_{16}H_{24}O_{12}NO_3^-$	470.115
$C_{16}H_{27}NO_{11}NO_3^-$	471.147
$C_{16}H_{26}O_{12}NO_3^-$	472.131
$(C_2H_7N)_4(H_2SO_4)_2HSO_4^-$	473.126
$C_{15}H_{27}NO_{12}NO_3^-$	475.142
<del><math>(H_2O)_2(NH_3)_3(H_2SO_4)_3HSO_4^-</math></del>	<del>477.963</del>



56 **Table S2** continued

Ion	Mass
<u><math>(C_2H_7N)_2(H_2SO_4)_3HSO_4^-</math></u>	<u>480.978</u>
$C_{17}H_{25}NO_{11}NO_3^-$	481.131
$C_{18}H_{28}O_{11}NO_3^-$	482.152
$C_{17}H_{27}NO_{11}NO_3^-$	483.147
$C_{20}H_{26}N_2O_8NO_3^-$	484.157
$C_{20}H_{27}NO_9NO_3^-$	487.157
<u><math>(H_2SO_4)_4(NH_3)_2NO_3^-</math></u>	<u>487.911</u>
$C_{20}H_{29}NO_9NO_3^-$	489.173

57